A multi-model assessment for the 2006 and 2010 simulations under the Air Quality Model Evaluation International Initiative (AQMEII) phase 2 over North America: Part I. Indicators of the sensitivity of O_3 and $PM_{2.5}$ formation regimes

Patrick Campbell [a, *], Yang Zhang [a, *], Khairunnisa Yahya [a], Kai Wang [a], Christian Hogrefe [b], George Pouliot [b], Christoph Knote [c], Alma Hodzic [c], Roberto San Jose [d], Juan L. Perez [d], Pedro Jimenez Guerrero [e], Rocio Baro [e], Paul Makar [f]

[a] *Department of Marine, Earth, and Atmospheric Sciences, NCSU, Raleigh, NC 27695, USA*
[b] *ORD, U.S. EPA, Research Triangle Park, NC 27711, USA*
[c] *Atmospheric Chemistry Division, NCAR Earth System Laboratory, NCAR, Boulder, CO 80301, USA*
[d] *Computer Science School, Technical University of Madrid, Campus de Montegancedo, Boadilla del Monte, 28660 Madrid, Spain*
[e] *Department of Physics, University of Murcia, Ed. CIOyN, Campus de Espinardo, University of Murcia, 30100 Murcia, Spain*
[f] *Air Quality Research Division, Environment Canada, Toronto, Ontario M3H 5T4, Canada*

---

[*] Corresponding authors.
E-mail addresses: pccampb2@ncsu.edu (P. Campbell), yzhang9@ncsu.edu (Y. Zhang).

1. Introduction

Significant advancements over the last decade have been made in modeling the tropospheric pollutants ozone (O_3) and particulate matter with an aerodynamic diameter ≤ 2.5 μm ($PM_{2.5}$), including rapid development and application of 3-D online-coupled meteorology and air quality models (AQMs) (Y. Zhang, 2008; Baklanov et al., 2014). Online-coupled AQMs allow for more detailed studies of the feedbacks between air quality and the climate/meteorology system (Y. Zhang et al., 2010, 2012a). AQMs such as the Community Multiscale Air Quality (CMAQ) (Byun and Schere, 2006) model, the Weather Research and Forecasting model with Chemistry (WRF/Chem) (Grell et al., 2005; Skamarock et al., 2008), and the Global Environmental Multi-scale Modelling Air Quality and Chemistry (GEM/MACH) (Moran et al., 2010) are used to model indicators of formation regimes, transport, and fate of O_3 and $PM_{2.5}$, thus providing regulatory decision-making value for the overall control of O_3 and $PM_{2.5}$ concentrations across the continental United States (U.S.) (Y. Zhang et al., 2009a,b; Liu et al., 2010).

AQMs need to be systematically evaluated using a common testbed/episode; however, unlike the global-scale climate modeling community, the regional-scale modeling communities in different continents, e.g., North America (NA) and Europe (EU), have begun such investigations only recently. Whereas Phase 1 of the Air Quality Modeling Evaluation International Initiative (AQMEII) focused on evaluation of regional scale, offline-coupled AQMs (Rao et al., 2011; Galmarini et al., 2012), AQMEII Phase 2 (AQMEII-2) placed its emphasis on evaluation of online-coupled AQMs utilizing common sets of time-dependent emissions and meteorological and chemical initial and boundary conditions, thus allowing for a diagnostic evaluation of inter-model discrepancies caused by specific model processes (Dennis et al., 2010). Such independent evaluations of regional-scale AQMs help place AQM results in context for the modeling community (e.g., Huijnen et al., 2010), while aiding their interpretation for future policy, regulation, and control decisions, with an overarching goal to improve our understanding of the connections between air quality and climate change (Alapaty et al., 2012).

Motivation to develop methods to diagnose the NO_x-VOC sensitivity, has led to significant development of "indicator-based" analyses, which are theoretically formulated from chemical reaction mechanisms and measurements of key gaseous species that lead to O_3 concentration changes in certain regions, and then applied to other regions where similar measurements are available by calculating the observation-based indicators, or to the regions where measurements are sparse through AQM simulations. These analysis methods use specific indicator quantities to determine the NO_x-VOC sensitivity of O_3 concentrations to precursor emission reductions (e.g., Milford et al., 1994; Sillman, 1995, 1999; Sillman et al., 1997, 1998; Lu and Chang, 1998; Tonnesen and Dennis, 2000; Hammer et al., 2002; Sillman and He, 2002; Martin et al., 2004; Liang et al., 2006). Previous modeling studies indicate that the ratio of production rates of hydrogen peroxide to nitric acid ($PH_2O_2/PHNO_3$), the concentration ratios of formaldehyde to total reactive nitrogen ($HCHO/NO_y$), and the ratios of the column abundances of HCHO to nitrogen dioxide ($HCHO/NO_2$) (Martin et al., 2004), are currently the most robust indicators (Y. Zhang et al., 2009b; Liu et al., 2010). Here we adopt 5 indicators from a compilation of studies along with their associated NO_x-VOC transition values summarized in Table 2 of Y. Zhang et al. (2009b). Specifically, the indicators (NO_x-limited transition values recommended by Y. Zhang et al. (2009b)) include H_2O_2/HNO_3 (≥ 2.4), $HCHO/NO_y$ (≥ 0.28), $HCHO/NO_2$ (≥ 1), NO_y (≤ 5), and O_3/NO_y (≥ 15). The simulations analyzed here did not include process analysis that calculates hourly values of PH_2O_2 and $PHNO_3$, and those productions rates are not included in the model output. The concentration ratio of H_2O_2/HNO_3 is thus used as a proxy for $PH_2O_2/PHNO_3$, although H_2O_2/HNO_3 is not as robust as $PH_2O_2/PHNO_3$.

A large fraction of secondary inorganic $PM_{2.5}$ in the troposphere is composed of sulfate (SO_4^{2-}), nitrate (NO_3^-), and ammonium (NH_4^+). Indicators for the complex interactions between the sensitivity of $PM_{2.5}$ concentrations to relations among total nitrate ($TN \equiv HNO_3 + NO_3^-$), total sulfate ($TS \equiv SO_4^{2-}$), and total ammonia ($TA \equiv NH_3 + NH_4^+$) have also been derived, tested, and implemented. From the work of Ansari and Pandis (1998), Pinder et al. (2008) derived a molar ratio known as the degree of sulfate neutralization ($DSN \equiv ([NH_4^+] - [NO_3^-])/[SO_4^{2-}]$), and used the DSN to express a refined gaseous free ammonia, NH_3^F ($NH_3^F \equiv TA - DSN \times TS$) and adjusted gas ratio, GR ($AdjGR \equiv NH_3^F/TN$), which are used as indicators of ammonia- and nitrate-limited regimes. Generally, in regions where the AdjGR is relatively large, sufficient gaseous NH_3 exists to neutralize SO_4^{2-}, and $PM_{2.5}$ NO_3^- concentrations are most sensitive to changes in TN. In regions of relatively smaller AdjGR, $PM_{2.5}$ NO_3^- concentrations are most sensitive to changes in NH_3. Here we adopt recommended transition values of DSN and AdjGR from Y. Zhang et al. (2009b), indicating the degree in which SO_4^{2-} has been neutralized by ammonium ($DSN \geq 1.5$; fully neutralized or $DSN < 1.5$; insufficiently neutralized), while determining NH_3 rich ($AdjGR > 1$) from NH_3 neutral/poor ($AdjGR \leq 1$) conditions. We also adopt two other molar ratios, TN/TS and TA/TS, which provide insight into NO_3^- poor ($TN/TS < 1$), medium ($TN/TS = 1–2$), or rich conditions ($TN/TS > 2$), and SO_4^{2-} rich ($TA/TS < 2$), neutral ($TA/TS = 2$), or poor ($TA/TS > 2$) conditions respectively (Y. Zhang et al., 2000, 2009b).

Extending the operational evaluation of O_3 and PM predictions against observations from surface monitoring stations for individual (e.g., Yahya et al., 2015a,b) and multiple models (e.g., Im et al., 2015a,b; Makar et al., 2015a,b) included in the AQMEII-2, this work further evaluates the models' performance in reproducing the selected indicators for O_3 and PM formation regimes and column predictions of gaseous mass abundance and aerosol and cloud properties for six AQMEII-2 participating groups. Such model evaluations complement traditional model evaluation that primarily focuses on surface O_3 and PM predictions, provide insights into the models' capability of probing into the underlying O_3 and PM formation mechanisms for emission control policy-making, and examine the interplay among chemistry, aerosol, and cloud through several feedback mechanisms, as well as the importance of upper boundary conditions in accurate predictions of column variables. These results are presented as a sequence of two parts. Part I describes the evaluation and inter-comparison of indicators of the sensitivity of O_3 and $PM_{2.5}$ formation regimes predicted by multiple model simulations against available surface and satellite observations, and the resulting policy implications. Part II describes the evaluation and inter-comparison of column mass abundance of gases and aerosol/cloud properties against satellite observations as well as potential model improvement in simulating chemistry-aerosol-cloud-climate feedbacks (Wang et al., 2015a). Main

Table 1
AQMEII-2 participating models and configurations for the North American domain simulations. The full citations for their italicized short-names are provided in the footnote (alphabetically) below the table.

	US8	US7	ES1	ES3	CA2f	US6
AQ-Meteo. model/ version	Modified WRF-Chem/ 3.4.1 *G05*, *Sk08*, *W14*	WRF-Chem/3.4.1 *G05*, *Sk08*	WRF-Chem/3.4.1 *G05*, *Sk08*	WRF-Chem/3.4.1 *G05*, *Sk08*	GEM-MACH/1.5.1 *M10*	WRF-CMAQ/5.0.1 *BS06*, *Fo10*, *W12*
Years	2006 & 2010	2010	2010	2006	2006 & 2010	2006 & 2010
Dx-Dy	36 km	36 km	36 km	36 km	15 km	12 km
Vertical resolution	35 eta levels	33 eta levels	33 eta levels	33 eta levels	58 eta levels	35 eta levels
1st layer height	38 m	60 m	29 m	18 m	21 m	19 m
Model top pressure	100 hPa	10 hPa	50 hPa	100 hPa	10 mb (2006), 0.1 hPa (2010)	100 hPa
Projection	Lambert	Lambert	Lambert	Lambert	Rotated Lat-Lon	Lambert
Domain center	39.3°N; 97.6°W	39.0°N; 97.5°W	39.0°N; 97.5°W	40.0°N; 97.0°W	n/a	40.0°N; 97.0°W
Meteo. ICs/BCs	NCEP FNL (1.0°)	NCEP FNL (1.0°)	NCEP GFS (1.0°)	NCEP GFS (1.0°)	GEM (15 km) – CMC *M06*,*Fi10*	NCEP NAM (12-km)
Chemical ICs/BCs	MACC-II *H08*, *S12*	MACC-II *H08*, *S12*	MACC-II *H08*, *S12*	MACC-II *H08*, *S12*	MACC-II *H08*, *S12*	MACC-II *H08*, *S12*
Land surface model	NOAH *CD01*, *Ek03*	NOAH *CD01*, *Ek03*	NOAH *CD01*, *Ek03*	NOAH *CD01*, *Ek03*	ISBA2 *B03*	Pleim-Xiu *XP01*
Surface layer	Monin-Obukhov *MO54*, *J02*	Monin-Obukhov *MO54*, *J02*	Monin-Obukhov *MO54*, *J02*	Monin-Obukhov *MO54*, *J02*	ISBA2 *B03*	Monin-Obukhov *MO54*, *J02*
PBL scheme	YSU *H06*	MYNN *NN04*	YSU *H06*	YSU *H06*	MOISTKE4 *MB82*, *B05*	ACM2 *P07*
Radiative transfer mech.	RRTMG *C05*	RRTM *M97*	RRTMG *C05*	RRTMG *C05*	*LB05*	RRTMG *C05*
Photolysis	FTUV *T03*	FTUV *T03*	Fast-J *W00*	Fast-J *W00*	ADOM-II *D72*, *P76*, *D88*	In-Line *B07*
Microphysics	Morrison *M09*	Morrison *M09*	Lin (Purdue) *L83*	Morrison *M09*	Milbrandt-Yao *MY05*	Morrison *M09*
Cloud paramet.	Grell 3D *GF13*	Grell 3D *GF13*	Grell 3D *GF13*	Grell 3D *GF13*	KF *KF90*	KF2 *K04*
Biogenic emissions	MEGAN *Gu06*	MEGAN *Gu06*	MEGAN *Gu06*	MEGAN *Gu06*	BEIS3.0.9 *P98*	BEIS3.14 *V02*, *S05*
Gas phase mech.	Modified CB05-Cl_x *Y05*, *S06*, *SB07*	MOZART-4 *Em10*, *K13*	RADM2 *S90*	CBMZ *Z99*	ADOMII *SL89*	CB05-TU *W10*
Aerosol mechanism/ size	MADE/3 modes *A98*, *G05*	MOSAIC/4 bins *Z08*	MADE/3 modes *A98*, *G05*	MOSAIC/4 bins *Z08*	CAM/12 bins *G03*	AERO6/3 modes *A13*
SOA mechanism	VBS *A12*	Hodzic and Jimenez *HJ11*	SORGAM *S01*	None	*O96*	CMAQ SOA *C10*, *S12*
Aqueous chemistry	CMAQ AQCHem *S11*	Grid and Sub-Grid *WT86*, *FP01*	Grid/Sub Grid *WT86*, *FP01*	Grid/Sub Grid *WT86*, *FP01*	ADOM *V88*, *F91*	Grid/Sub Grid
Dust & sea-salt scheme	Dust: AER/AFWA *JC11* Sea-salt: *G97*	Dust: MOSIAC *Sh08* Sea-salt: *G97*	Dust: MOSIAC *Sh08* Sea-salt: *G97*	Dust: MOSIAC *Sh08* Sea-salt: *G97*	Dust: None Sea-salt: *G03*	Dust: In-Line *A13* Sea-salt: In-Line *K10*
Aerosol direct effect	Fast-Chapman *F06*,*C09*	Fast-Chapman *F06*,*C09*	Fast-Chapman *F06*,*C09*	Fast-Chapman *F06*,*C09*	GEM-MACH Feedback *BH83*	CMAQ Feedback *BH98*, *W12*
Aerosol indirect effect	AR-G00 *ARG00*	AR-G00 *ARG00*	AR-G00 *ARG00*	AR-G00 *ARG00*	AR-G00 *ARG00*	None
Urban canopy	UCM *K01*	UCM *K01*	None	None	None	None
Wet deposition	Grid/Sub-Grid *E04*	Grid/Sub-Grid *E04*	Grid/Sub-Grid *E04*	Grid/Sub-Grid *E04*	AURAMS *Go06*	CMAQ *WT86*, *BS06*
Dry deposition	Gases: Wesely *W89*, *WH00*, *Z02* Particles: CMAQ – *BS95*	Gases: Wesely *W89*, *WH00*, *Z02* Particles: MOSAIC Driven	Gases: Wesely *W89*, *WH00*, *Z02* Particles: MADE Driven	Gases: Wesely *W89*, *WH00*, *Z02* Particles: MOSAIC Driven	Gases: Wesley Particles: *G03[a]*, *Z01*	Gases & Particles: CMAQ In-Line *P01*, *PR11*

References: ARG00 – Abdul-Razzak and Ghan (2000); A98 – Ackerman et al. (1998); A12 – Ahmadov et al. (2012); A13 – Appel et al. (2013); B03 – Belair et al. (2003a,b); B05 – Belair et al. (2005); BS95 – Binkowski and Shankar (1995); B07 – Binkowski et al. (2007); BH83 – Bohren and Huffman (1983); BH98 – Bohren and Huffman (1998); BS06 – Byun and Schere (2006); C10 – Carlton et al. (2010); C09 – Chapman et al. (2009); CD01 – Chen and Dudhia (2001); C05 – Clough et al. (2005); D72 – Dave (1972); D88 – DeMore et al. (1988); E04 – Easter et al. (2004); Ek03 – Ek et al. (2003); Em10 – Emmons et al. (2010); FP01 – Fahey and Pandis (2001); F06 – Fast et al. (2006); Fi10 – Filion et al. (2010); Fo10 – Foley et al. (2010); F91 – Fung et al. (1991); G97 – Gong et al. (1997); G03 – Gong et al. (2003a,b); Go06 – Gong et al. (2006); G05-Grell et al. (2005); GF13 – Grell and Frietas (2013); Gu06 – Guenther et al. (2006); HJ11 – Hodzic and Jimenez (2011); H08 – Hollingsworth et al. (2008); H06 – Hong et al. (2006); J02 – Janjic (2002); JC11 – Jones and Creighton (2011); KF90 – Kain and Fritsch (1990); K04 – Kain (2004); K10 – Kelly et al. (2010); K13 – Knote et al. (2013); K01 – Kusaka et al. (2001); LB05 – Li and Barker (2005); L83 – Lin et al. (1983); MB82 – Mailhot and Benoit (1982); M06 – Mailhot et al. (2006); MY05 – Milbrandt and Yao (2005a,b); M97 – Mlawer et al. (1997); MO54 – Monin and Obukhov (1954); M10 – Moran et al. (2010); M09 – Morrison et al. (2009); NN04 – Nakanishi and Niino (2004); O96 – Odum et al. (1996); P76 – Peterson (1976); P98 – Pierce et al. (1998); P01 – Pleim et al. (2001); P07 – Pleim (2007a,b); PR11 – Pleim and Ran (2011); S06 – Sarwar et al. (2006); SB07 – Sarwar and Bhave (2007); S11 – Sarwar et al. (2011); S01 – Schell et al. (2001); S12 – Schere et al. (2012); S05 – Schwede et al. (2005); Sh08 – Shaw et al. (2008); SB12 – Simon and Bhave (2012); Sk08 – Skamarock et al. (2008); SL89 – Stockwell and Lurmann (1989); S90 – Stockwell et al. (1990); T03 – Tie et al. (2003); V88 – Venkatram et al. (1988); V02 – Vukovich and Pierce (2002); WT86 – Walcek and Taylor (1986); W14 – Wang et al. (2015b); W89 – Wesely (1989); WH00 – Wesely and Hicks (2000); W10 – Whitten et al. (2010); W00 – Wild et al. (2000); W12 – Wong et al. (2012); XP01 – Xiu and Pleim (2001); Y05 – Yarwood et al. (2005); Z99 – Zaveri and Peters (1999); Z08 – Zaveri et al. (2008); Z01 – L. Zhang et al. (2001); Z02 – L. Zhang et al. (2002).

objectives of this Part I paper are to perform an operational evaluation, investigatory/diagnostic, and dynamic analysis (Y. Zhang et al., 2006; Dennis et al., 2010) of four 2006 and five 2010 simulations with three online-coupled AQMs (WRF/Chem, WRF/CMAQ and GEM/MACH) for a NA domain, with a focus on the selected indicators that probe into the sensitivity of O_3 and $PM_{2.5}$ formation regimes in NA, specifically for U.S. sub-regions. Specifically, we will 1) assess the models' accuracy against surface and satellite observations, 2) compare seasonal inter-model differences in spatial and temporal (2006–2010) variability, 3) discuss potential reasoning for any model biases and differences, and 4) use the results from 1) – 3) to assess the robustness of the different indicators used in policy-making decisions, while demonstrating a need for increasing measurements and modeling of O_3 and $PM_{2.5}$ indicators, which would further serve to impact future policy-making.

2. AQMEII-2 model configurations, observations, and evaluation protocols

2.1. AQMEII-2 configurations and input

Table 1 summarizes the six AQMEII-2 participating models over NA in this study (four from NA and two from EU), and their model configurations. Those models include US8, US7, ES3, CA2f, and US6. US8, US7, ES1, and ES3 are based on WRF/Chem version 3.4.1 or its variant (Wang et al., 2015b), CA2f is the GEM/MACH version 1.51 (Moran et al., 2010), and US6 is the two-way coupled WRF/CMAQ version 5.0.1 with aerosol direct effect only (Wong et al., 2012).

Each model uses the same time-resolved emissions and chemical initial and boundary conditions (ICs and BCs respectively). Emissions are comprised of data from the U.S., Canada, and Mexico. For the U.S. emissions, the 2008 National Emission Inventory (NEI) (version 2, released April 10, 2012) was used as the basis for both the 2006 and 2010 model ready emission datasets (http://www.epa.gov/ttn/chief/net/2008inventory.html) (Pouliot et al., 2015). The 2008-based modeling platform (2007v5 in final form dated 12/14/2012; http://www.epa.gov/ttn/chief/emch/index.html#2008) provided all necessary inputs and datasets for emission processing (Pouliot et al., 2015). These files contain the chemical speciation files, the temporal allocation, and spatial allocation data. A technical support document (2007v5 Emissions Platform Technical Support Document-12/14/2012) is available for this modeling platform, and contains the full details of the inventory preparation and processing. Year specific (2006 and 2010) updates for these sectors were used for on/off road transport, wildfires and prescribed fires, and Continuous Emission Monitoring (CEM)-equipped point sources. There are widespread decreases in SO_2, NO_x, and NH_3 emissions between 2006 and 2010 across the NA domain, with the exception of some large NH_3 emission increases in the Midwestern U.S. and California in winter (Pouliot et al., 2015; Yahya et al., 2015b). Dependent on the region of the NA domain and season considered, there were both increases (summer and fall in southeast U.S.) and decreases (winter and spring across most of U.S.) in VOC emissions between 2006 and 2010 (Pouliot et al., 2015; Yahya et al., 2015b). The chemical 2006 and 2010 ICs and BCs are from global 3-h Monitoring Atmospheric Composition and Climate – Interim Implementation (MACC-II; http://www.gmes-atmosphere.eu/) fields (Inness et al., 2013). Further details regarding both the 2006–2010 emission and IC and BC changes for the AQMEII-2 NA domain are found in this issue (Pouliot et al., 2015; Stoeckenius et al., 2015; Yahya et al., 2015b).

There are many similarities and differences in model configurations across the participating groups (Table 1). US8, US7, ES1, and ES3 share the most similar configurations available in WRF/Chem, and employ the same horizontal resolution of 36 × 36 km; although there is at least one configuration difference between each model. There are more differences than similarities among those WRF/Chem-based models, compared to the CA2f and US6 configurations. CA2f and US6 also utilize finer horizontal resolutions of 15 × 15 km and 12 × 12 km, respectively. Important for diagnosing model differences in O_3 and inorganic $PM_{2.5}$ indicators, all groups employ different gas-phase mechanisms, as well as different combinations of gas-phase and aerosol mechanisms. Inter-model comparisons in Section 4 use such similarities and differences as a basis for investigatory/diagnostic analyses.

2.2. Observations from surface networks and satellites

Observations from both surface and satellite platforms are used for the evaluation. For a detailed site-specific comparison, surface observations from the SouthEastern Aerosol Research and Characterization (SEARCH) network (Hansen et al., 2003) are used. This is an ideal network for comparison, as it readily provides coincident measurements of trace gas and particulate species necessary to calculate the surface O_3/NO_y indicator, and $PM_{2.5}$ indicators such as DSN, AdjGR, and NH_3^F. With the exception of specific field campaigns, such routine measurement combinations are sparse for other regions of the U.S., especially for gas-phase NH_3 and HNO_3, which is needed for calculating $PM_{2.5}$ indicators AdjGR and NH_3^F. From the SEARCH network, four sites are selected from urban/suburban locations, Birmingham, Alabama (BHM), Jefferson Street, Atlanta (JST), Gulfport, Mississippi (GFP), and the Outlying Landing Field #8, Florida (OLF). Three sites are also selected from rural areas, Centreville, Alabama (CTR), Yorkville, Georgia (YRK), and Oak Grove, Mississippi (OAK). Full descriptive information regarding the SEARCH network, including each site's location, descriptive information, and relevant measurements necessary for calculations of O_3 and $PM_{2.5}$ indicators in 2006 and 2010, may be found at http://www.atmospheric-research.com/. Tropospheric column observations of level-3 monthly averaged NO_2 and HCHO data are also obtained from the Scanning Imaging Absorption Spectrometer for Atmospheric Chartography (SCIAMACHY) (Boersma et al., 2004; De Smedt et al., 2008), and are used for a domain-wide evaluation of the column $HCHO/NO_2$ indicator (Martin et al., 2004). SCIAMACHY column NO_2 and HCHO data have been validated and applied in previous investigations (e.g., van der A et al., 2006, 2008; Barkley et al., 2013).

2.3. Evaluation protocols

Following Y. Zhang et al. (2009a), our protocol includes an evaluation between model and observations using different statistical measures, and a diagnostic/dynamic evaluation of model inter-comparisons for the investigation of process-based differences and systematic biases on a seasonal and regional basis. Simulated O_3 and $PM_{2.5}$ indicators are compared against observations from the SEARCH locations in southeast U.S., using the closest horizontal grid values, at the vertical layer closest to the surface for each model (Table 1). We note that this is similar to a case study based evaluation limited to southeast U.S. In light of this, Section 5 of this paper provides additional discussion on the benefits, limitations, and recommendations regarding this evaluation. Statistical measures typically used to evaluate AQMs are implemented here. These include the normalized mean bias (NMB), normalized mean error (NME), and Pearson's correlation coefficient, R (Y. Zhang et al., 2006). Statistical measures R, NMB, and NME provide measures of the associativity (i.e., correlation), bias, and accuracy, respectively, of specific modeled surface O_3 and $PM_{2.5}$ indicators. A model spatial and statistical (NME vs. NMB) comparison of the tropospheric column $HCHO/NO_2$ (Martin et al., 2004) indicator is also made against SCIAMACHY satellite observations for the O_3 (May–September) and non-O_3 (January–April and October–December) seasons. The hour during the orbit crossing-time of SCIAMACHY is ~10:00 a.m. local time. The model results from 1500 to 2000 UTC are averaged to approximately match the 10:00 local time of the SCIAMACHY observations (Wang et al., 2015a). Modeled HCHO and NO_2 column abundances are determined by vertically integrating up to the tropopause, which is assumed to be 100 hPa following Y. Zhang et al. (2009a), while also cloud screening the model output using a 40% cloud fraction threshold that is consistent with the SCIAMACHY retrieval (De Smedt et al., 2008). Considering that an averaging kernel is not available for the level-3 SCIAMACHY data used in this comparison, an averaging kernel is not applied to the model data. Our calculation of the model column HCHO and NO_2 abundances represents an approximate comparison of the tropospheric amounts to match the satellite data. Thus the model-satellite matching, as well as the model and SCIAMACHY column data, is subject to uncertainties. More details in regards to the uncertainties and limitations associated with SCIAMACHY column HCHO and NO_2 ratios data are found in Wang et al. (2015a).

Diagnostic/dynamic inter-model comparisons are performed by analyzing the seasonal variation of the spatial distribution of indicators and investigating process-based reasoning due to model configuration differences (Table 1), as well as different model responses to changes in emissions and meteorology between the 2006 and 2010 simulations. Analyses and comparisons are based on a geographical separation into 4 sub-regions across NA, which have been defined in Solazzo et al. (2012a,b). Adapting a similar definition, henceforth we refer to NA1, NA2, NA3, and NA4 as the west (120–105°W/30–50°N), Midwest (105–90°W/30–50°N), southeast (90–75°W/25–40°N), and northeast (90–65°W/40–50°N) regions of the NA domain respectively. The entire continental U.S. region of the NA domain, i.e., NA/U.S. is approximated using the areas encompassed by sub-regions NA1-NA4.

3. Evaluation of simulated indicators against observations

3.1. O_3/NO_y statistical comparison

Fig. 1 provides statistical plots (NMB vs. NME) for simulated O_3/NO_y indicator ratios against those calculated based on the averaged SEARCH observations of O_3 and NO_y in 2006 (ES3), 2010 (US7 and

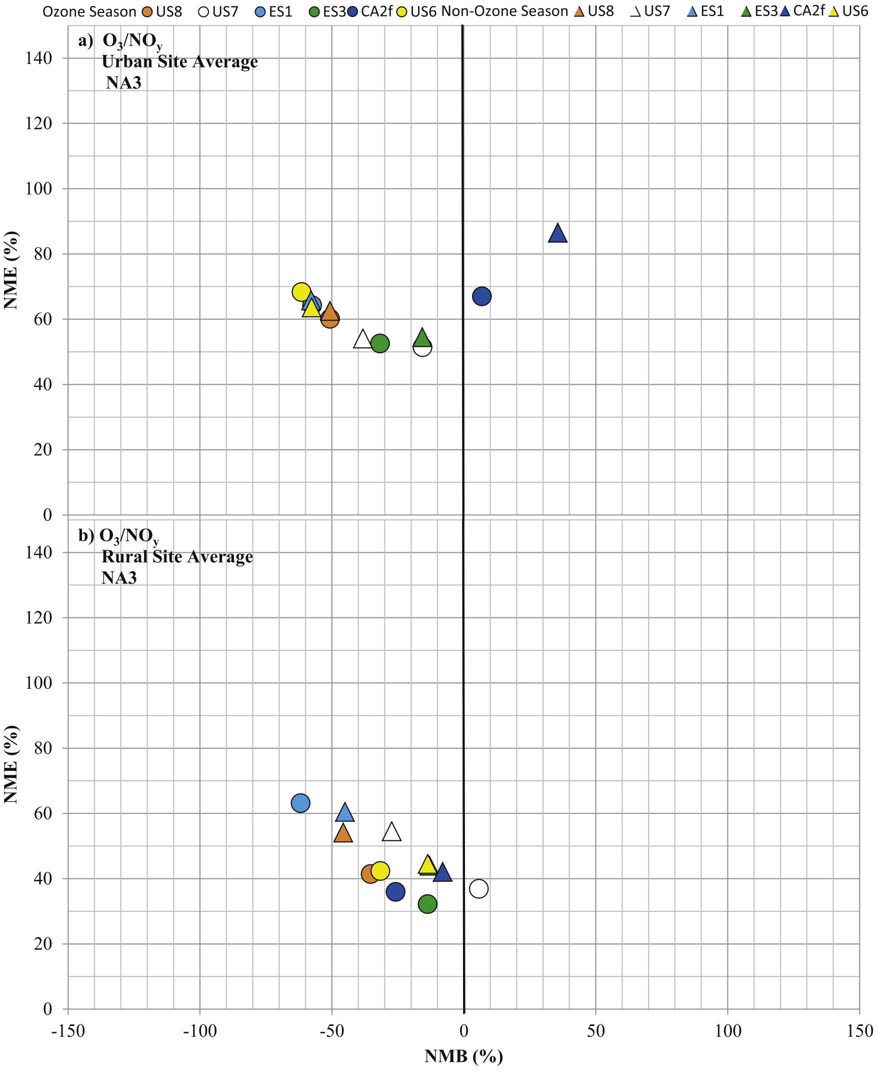

Fig. 1. Averaged NMB and NME for modeled O_3/NO_y against SEARCH observations averaged over the urban (a) and a rural sites (b) in NA3. Colored circles and triangles pertain to the model's average values over O_3 and non-O_3 seasons, respectively. (For interpretation of the references to color in this figure legend, the reader is referred to the web version of this article.)

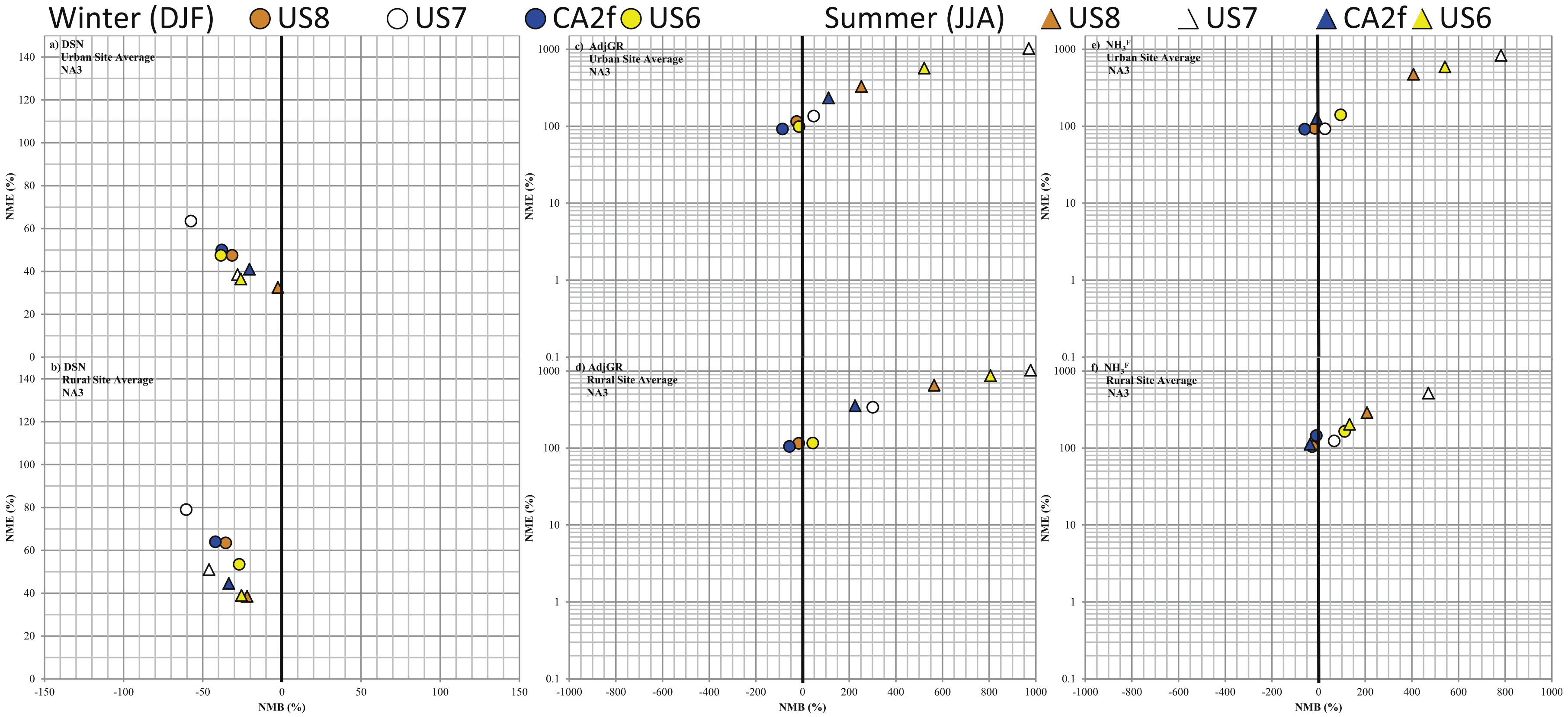

Fig. 2. Averaged NMB and NME for the comparison of the modeled DSN (a, b), AdjGR (c, d), and NH$_3^F$ (e, f) against SEARCH observations averaged over the urban (top) and a rural sites (bottom) in NA3. Colored circles and triangles pertain to the model's average values over O$_3$ and non-O$_3$ seasons, respectively. (For interpretation of the references to color in this figure legend, the reader is referred to the web version of this article.)

ES1), or the average of 2006 and 2010 (US8, CA2f, and US6), for afternoon hours (1 p.m.–6 p.m. LST) during the O_3 and non-O_3 seasons in the southeast U.S., NA3. There is predominantly a negative O_3/NO_y bias for the models, especially at the rural sites (Fig. 1b). The negative O_3/NO_y bias for the models is dominated by an overprediction in NO_y, except for CA2f which has an underprediction in NO_y (Figure S1), and a positive O_3/NO_y bias at the urban sites during both seasons (Fig. 1a). More details regarding the model predictions of O_3 and NO_y individually, and their underlying causes, are found in comparisons against four SEARCH sites in Supplementary Section 1 and Figure S1. US6 and US8 have the highest correlation coefficient, R (not shown), while ES3 and US7 have the smallest bias and error in NO_x-VOC sensitivity for the urban sites (Fig. 1a), i.e., they have the most similar distance to the linear transition line compared to observations in Figure S1. At the rural sites, there is generally less error (Fig. 1b), while US7 and CA2f have the smallest bias and error during the O_3 and non-O_3 seasons respectively. On average across both seasons, the most finely resolved US6 model (12 × 12 km) has the highest correlation (not shown), and best represents local changes in the O_3/NO_y ratio in NA3.

For the models at the urban sites, the NMB for O_3/NO_y ranges from −62% to +6.9% in the O_3 season, and from −58% to +36% in the non-O_3 season. At the rural sites, the models' NMB range is −62% to +5.7%, and −46% to +8% in the O_3 and non-O_3 season, respectively.

Future improvement in the models' predominant overprediction of NO_y is needed to reduce the predominant negative O_3/NO_y bias, and the overprediction in VOC-limited extent of O_3 chemistry in NA3.

3.2. *DSN, AdjGR, and NH_3^F statistical comparison*

Fig. 2 provides NMB vs. NME plots for DSN, AdjGR, and NH_3^F indicators against SEARCH observations in NA3 for the 2010 (US8, US7, CA2f, and US6) winter and summer seasons. Supplementary Section 2 and Figure S2 provide additional details for each model's average $PM_{2.5}$ regime indicators TA/TS, TN/TS, DSN, AdjGR, and NH_3^F, compared to four SEARCH sites during all seasons in 2010. Although ES1's simulation is included in the analyses in Section 3.1 (see additional discussion in Supplementary Section 1), exclusion of SO_2 and NO_x point sources for ES1 led to unrealistic concentrations of inorganic $PM_{2.5}$ species. Thus ES1's results are not included in Fig. 2 and subsequent figures comparing $PM_{2.5}$ indicators. For all models, seasons, and sites the correlation coefficient, R (not shown), is very low for all indicators, and at times negative. This illustrates the difficulty for models to capture observed trends in $PM_{2.5}$ regime indicators at individual sites; although higher statistical scores may be found for individual particle species when larger numbers of stations are included in the analysis (Table 4 in Makar et al., 2015a). All models predict a negatively biased DSN at both urban and rural sites, thus underestimating SO_4^{2-} neutralization by ammonium in both seasons (Fig. 2a and b). The US8 model has the smallest DSN bias and error, on average, during the winter and summer at the urban sites. At the rural sites, US6 and US8 have the smallest bias and error in the winter and summer, respectively. Given model overpredictions of NH_3 and TA (not shown), a negatively biased DSN, and impacts from uncertainties in NO_x emissions leading to underpredictions in TN, the result is a majority of very large positive biases and error for AdjGR and NH_3^F at both urban and rural sites, especially in the summer (Fig. 2c–f). There is also significantly more spread across the models for the positive biases in the summer. CA2f has consistently the lowest bias and error for AdjGR and NH_3^F during the summer at both urban and rural sites, which is due to partial compensation from large underpredictions in NO_2 concentrations (Table S1 in Makar et al., 2015a). For the winter, US6 and US8 have the smallest magnitudes in bias and error.

For the models at the urban sites, the NMB for DSN, AdjGR, and NH_3^F have ranges of −58% to −32%, -86% to +48%, and −60% to +95% in the winter season, and −28% to −2.5%, +112% to +970%, and −8% to +782%, during the summer season, respectively. There is a large NMB range for AdjGR and NH_3^F, and largely positive NMB during the summer season. In both the winter and summer seasons at urban sites, there is an overprediction in the extent of NH_3 rich conditions, and associated $PM_{2.5}$ sensitivity to TN changes. There are similar large ranges at the rural sites, where the model range NMB for DSN, AdjGR, and NH_3^F are −61% to −27%, -56% to +300%, and −37% to +112% during the winter season, and −46% to −26%, +226% to +978%, and −37% to +471% during the summer season respectively. There is clearly more error and bias when simulating $PM_{2.5}$ indicators, relative to the O_3 indicators in Section 3.1. Much of the additional model uncertainty for $PM_{2.5}$ indicators, especially for AdjGR, stems from additional complexities of accurately predicting thermodynamic partitioning for different species, uncertainties in gas emissions and meteorological conditions, as well as approximations contained within each model's gas-phase and aerosol module combinations.

3.3. *Satellite $HCHO/NO_2$ statistical comparison*

Fig. 3 provides NMB vs. NME plots for tropospheric $HCHO/NO_2$ column abundance ratio (Martin et al., 2004) against SCIAMACHY observations, averaged across the approximated continental U.S. (NA/U.S.), and over sub-regions in northwest (NA1), Midwest (NA2), southeast (NA3), and northeast U.S. (NA4), in 2006 (ES3), 2010 (US7 and ES1), or the average of 2006 and 2010 (US8, CA2f, and US6) O_3 and non-O_3 seasons. More details regarding the spatial agreement for each model against SCIAMACHY observations can be found in Supplementary Section 3 and Figure S3. For NA/U.S. (Fig. 3a), there is a negative $HCHO/NO_2$ bias for both seasons, with the exception of positive biases for ES1 and CA2f during the O_3 season. The underprediction in the NO_x-limited chemistry is mainly due to lower HCHO in rural regions, and larger NO_2 in urban regions. The NO_x-limited underprediction is apparent for all models and seasons in sub-region NA1 (Fig. 3b), except ES1 and CA2f in the O_3 season, covering the western U.S domain. In fact, during the non-O_3 season, there is a clear NO_x-limited underprediction in all NA/U.S. sub-regions (Fig. 3b–e) for the models, with the exception of ES1 and CA2f in NA2 and NA3. In NA2 (Fig. 3c) and NA3 (Fig. 3d) during the O_3 season, however, most models actually have a relatively slight overprediction of the NO_x-limited chemistry, due to overpredictions in HCHO concentration. There are significant contributions from underpredictions in NO_2, and hence NO_x concentrations for CA2f (Makar et al., 2015a), as well as known impacts from exclusion of NO_x point sources for ES1 during the O_3 season. Such NO_x underpredictions for ES1 and CA2f cause these models to be outliers for NA/U.S. and all sub-regions. When ES1 and CA2f are not considered, the models' NMBs for the O_3 season in NA1, NA2, NA3, NA4, and NA/U.S. range from −49% to −34%, +12% to +21%, -20% to +36%, -36% to −26%, and −32% to −15%, respectively. In the non-O_3 season, NMBs range from −93% to −90%, -82% to −31%, -55% to −7%, -99% to −92%, and −96% to −78% respectively. With exception of ES1 and CA2f, the models predominantly underpredict the extent of NO_x-limited chemistry for the column $HCHO/NO_2$ indicator, except in parts of NA2 and NA3, Canada, Mexico and the Atlantic Ocean (Figure S3), where there is a tendency to overpredict NO_x-limited chemistry in the O_3 season.

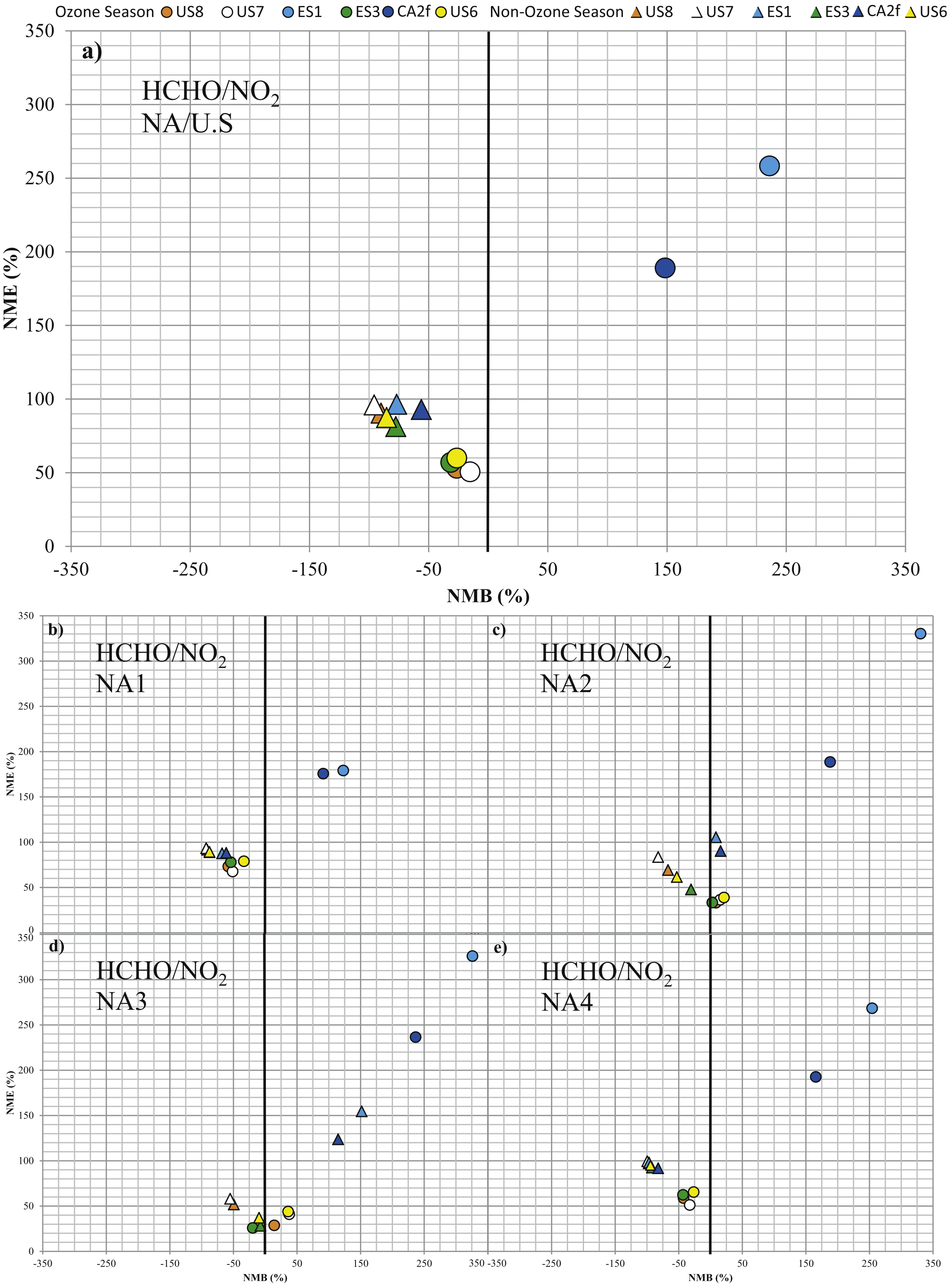

Fig. 3. Averaged NMB and NME for the comparison of modeled HCHO/NO$_2$ against SCIAMACHY observations averaged over the (a) NA/U.S., and sub-regions (b) NA1, (c) NA2, (d) NA3, and (e) NA4. Colored circles and triangles pertain to the model's average values over O$_3$ and non-O$_3$ seasons, respectively. (For interpretation of the references to color in this figure legend, the reader is referred to the web version of this article.)

4. Spatial distribution of seasonally averaged indicators

This section performs an inter-model comparison using ensemble model averages, standard deviations (SD), and normalized standard deviations (NSD = standard deviation/average) of the different NO_x-VOC-limited indicators during the O_3 season (Section 4.1), regime indicators for the formation of $PM_{2.5}$ in the winter (Section 4.2), and the inter-model changes between 2006 and 2010 (Section 4.3). Supplementary Section 4 provides additional details of the inter-model spatial comparisons, and further supplements the analyses in the following sections. The CA2f model did not contain H_2O_2 in its output, and thus the H_2O_2/HNO_3 indicator for CA2f is not included in these analyses.

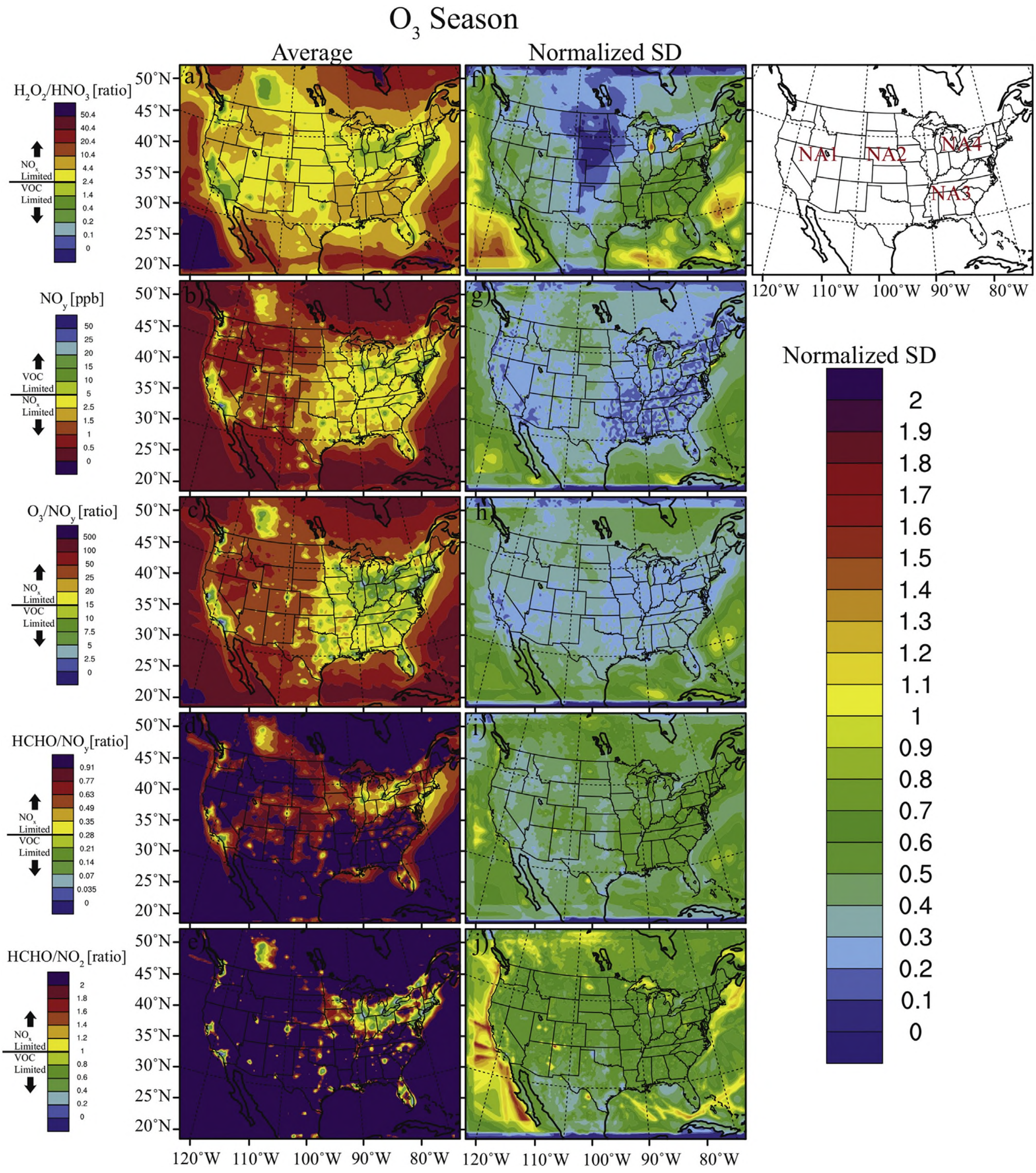

Fig. 4. Ensemble model average and normalized standard deviation of surface H_2O_2/HNO_3, NO_y, O_3/NO_y, $HCHO/NO_y$, and $HCHO/NO_2$, for average afternoon hours, during the O_3 season (May–September). Average NO_x-VOC-limited chemistry indicator value (a–e) is color shaded according to the legends on the left, while the normalized standard deviation's (f–j) color shading corresponds to the legend on the right. The panel in the top right shows the geographical sub-regions of NA used for discussion in the text. (For interpretation of the references to color in this figure legend, the reader is referred to the web version of this article.)

4.1. NO_x-VOC sensitivity in the O_3 season

Fig. 4 shows the ensemble model average and NSD of the five surface photochemical indicators (H_2O_2/HNO_3, NO_y, O_3/NO_y, $HCHO/NO_y$, and $HCHO/NO_2$), averaged over afternoon hours (1 p.m.–6 p.m. LST) during the O_3 season. For the H_2O_2/HNO_3 indicator (Fig. 4a), on average the models predict NO_x-limited chemistry in NA1, NA2, and NA4, with local areas of VOC-limited chemistry near urban centers. Models best agree in the relatively low biogenic emission region of NA2, which has the lowest NSD for H_2O_2/HNO_3; however, there are larger NSDs in the relatively high biogenic emission region of NA3 (Fig. 4f). Table 2 indicates average SDs of 1.18 and 3.13 and NSDs of 0.29 and 0.62 for H_2O_2/HNO_3 in NA2 and NA3, respectively. The higher inter-model variability in NA3 are due to differences in regional background H_2O_2 mixing ratios (~factor of 2; not shown), stemming from application of different gas-phase chemistry mechanisms between the models (Table 1). ES3 incorporates a different version of the Carbon Bond Mechanism (CBM), CBM-Z, compared to both US8 and US6 that use an updated CBM, i.e., CB05, while US7 uses a non-CBM (Table 1). Compared to CBM-Z, CB05 includes additional species such as higher aldehyde and internal olefin species, which increase radical production; it also explicitly defines methylperoxy radicals (Yarwood et al., 2005). Thus larger H_2O_2 may be attributed to gas-phase chemistry updates in CB05, and also differences between CBM and non-CBM (US7 and ES1) treatments (Table 1). Knote et al. (2015) conducted a diagnostic evaluation of the different chemical mechanisms used here in a box modeling approach, and their results support this suggestion.

For NO_y (Fig. 4b) and O_3/NO_y (Fig. 4c), there is also dominant NO_x-limited chemistry across NA/U.S., and local areas of VOC-limited chemistry near major urban centers. There are lower NSDs and better agreement across the models for the NO_y (Fig. 4g) and O_3/NO_y (Fig. 4h) indicators compared to H_2O_2/HNO_3. In NA3 the average SDs are 0.88 ppb and 4.33 and NSDs are 0.23 and 0.31 for NO_y and O_3/NO_y, respectively. These NSDs are about a factor of two lower than those for H_2O_2/HNO_3 in this region (Table 2). There is disparity across different model resolutions, however, when comparing the magnitude of NO_y for the different models at local areas (Supplementary Figure S4g–S4l), consistent with the comparison at local SEARCH sites, and the apparent spread in NO_y mixing ratios among models (Figure S1). ES1 agrees well for NO_y, but is biased low compared to other models for O_3/NO_y (Figure S4o). This is due to the impacts from exclusion of NO_x point sources important to O_3 formation. A negative O_3 bias for ES1 is apparent in other AQMEII-2 evaluations as well (Im et al., 2015a).

For $HCHO/NO_y$ (Fig. 4d) and $HCHO/NO_2$ (Fig. 4e) indicators, the model average also indicates strongly NO_x-limited conditions in NA/U.S. (dominated by the non-CBM model values; Figure S4). There is significant inter-model variability for these indicators, and relatively larger average NSDs across NA/U.S. (Fig. 4i–j), especially for $HCHO/NO_2$. The NSDs are the largest, 0.58, for $HCHO/NO_y$ in NA3, and 0.66, for $HCHO/NO_2$ in NA4 (Table 2). This is attributed to different biogenic emission models and versions employed for different models (Table 1; MEGAN2 vs. BEIS3.09 vs. BEIS3.14), combined with different gas-phase chemistry mechanisms, especially for the CBM versus non-CBM treatments. Better inter-model and observational agreement for US6 compared to CA2f (Fig. 3 and S4y-S4dd), may also be impacted by updated biogenic emission factors and treatment of light correction factors for isoprene (Schwede et al., 2005) used in conjunction with recent organic chemistry updates in CB05-TU for US6. Both CA2f and ES1, however, are also impacted by low NO_x concentrations (discussed above), and this contributes to their inter-model differences in $HCHO/NO_y$ and $HCHO/NO_2$. Significant differences near urban centers may also similarly be attributed to differences in organic chemistry treatment in the non-CBM gas-phase chemistry for US7, ES1, and CA2f (Table 1). Box model simulations for Detroit metro emissions indicate that the non-CBM mechanism for CA2f (ADOMII; Table 1) is ~100% larger than the CBM for US8 and US6 (CB05; Table 1) for HCHO, and ~50% lower for NO_x (Knote et al., 2015). This agrees with the $HCHO/NO_y$ differences near urban centers shown here. Comparison of the tropospheric column $HCHO/NO_2$ (Figures S3a–S3g) to surface $HCHO/NO_2$ (Figures S4y–S4dd) in the O_3 season indicates a similar spatial distribution in formation regimes; however, there are less VOC-limited regions near the urban centers for the column $HCHO/NO_2$ indicator, as well as more widespread NO_x-limited regimes. The impact of local NO_x sources is dampened when using the column $HCHO/NO_2$ indicator, as the NO_2 concentration is dominated by surface emissions, while the HCHO in the free troposphere is controlled by methane oxidation (Lowe and Schmidt, 1983; Wuebbles and Hayhoe, 2002; Palmer et al., 2003). Given the long lifetime of methane, the HCHO column is relatively well mixed (Fig. 1 in Li et al., 2012) compared to the NO_2 column.

Table 2
Statistical summary of the NA1, NA2, NA3, NA4, and NA/U.S.-wide ensemble model average, standard deviation, and normalized standard deviation (standard deviation/average) for each O_3 and $PM_{2.5}$ indicator in the O_3 and winter (DJF) seasons respectively.

Indicator	H_2O_2/HNO_3	NO_y	O_3/NO_y	$HCHO/NO_y$	$HCHO/NO_2$	TN/TS	DSN	AdjGR	NH_3^F	NO_3^-
Region	Ratio	ppb	Ratio	Ratio	Ratio	Ratio	Ratio	Ratio	ppb	$\mu g\ m^{-3}$
Average										
NA1	4.15	1.36	39.22	0.93	5.33	2.27	1.33	1.12	0.45	0.29
NA2	4.10	2.06	24.32	0.97	3.24	2.61	1.53	1.92	1.04	1.02
NA3	5.09	3.83	13.94	1.01	2.85	2.35	1.38	1.05	0.83	1.16
NA4	4.91	3.04	23.78	0.81	3.19	2.29	1.05	1.10	0.53	0.93
NA/U.S.	4.57	2.57	25.31	0.93	3.66	2.38	1.32	1.30	0.71	0.85
Standard Deviation (SD)										
NA1	1.49	0.42	12.99	0.41	3.34	1.29	0.38	0.69	0.18	0.14
NA2	1.18	0.64	8.13	0.47	1.88	1.21	0.37	1.39	0.40	0.61
NA3	3.13	0.88	4.33	0.58	1.79	1.22	0.31	0.85	0.37	0.65
NA4	2.14	0.84	8.19	0.41	2.11	1.42	0.45	1.14	0.31	0.66
NA/U.S.	1.94	0.72	8.36	0.47	2.28	1.29	0.39	1.03	0.33	0.50
Normalized Standard Deviation (NSD)										
NA1	0.36	0.31	0.33	0.44	0.63	0.57	0.28	0.62	0.40	0.48
NA2	0.29	0.31	0.33	0.48	0.58	0.46	0.24	0.72	0.38	0.60
NA3	0.62	0.23	0.31	0.57	0.63	0.52	0.23	0.81	0.45	0.56
NA4	0.44	0.28	0.34	0.51	0.66	0.62	0.43	1.04	0.59	0.70
NA/U.S.	0.42	0.28	0.33	0.50	0.62	0.54	0.30	0.80	0.46	0.59

This impact is especially apparent where there is already known deficiencies in NO_x concentrations for ES1 and CA2f. Thus the predicted NO_x-VOC limited regimes are dependent upon either using a modeled surface or column $HCHO/NO_2$ indicator to predict NO_x-versus VOC-limited regimes in NA/U.S. The NSDs for NA/U.S. in Table 2 indicate relatively small inter-model variability for NO_y (0.28) and O_3/NO_y (0.33) indicators, but larger inter-model variability for $HCHO/NO_y$ (0.50) and $HCHO/NO_2$ (0.62). The lowest inter-model variability is for NO_y in NA3 (0.23), while the largest is for $HCHO/NO_2$ in NA4 (0.66). Based on these results, the NO_y and O_3/NO_y indicators are the most robust.

4.2. *$PM_{2.5}$ sensitivity in winter*

Fig. 5 shows the ensemble model average and NSD of TN/TS, DSN, AdjGR, NH_3^F, and NO_3^- in winter (DJF), as this season is when

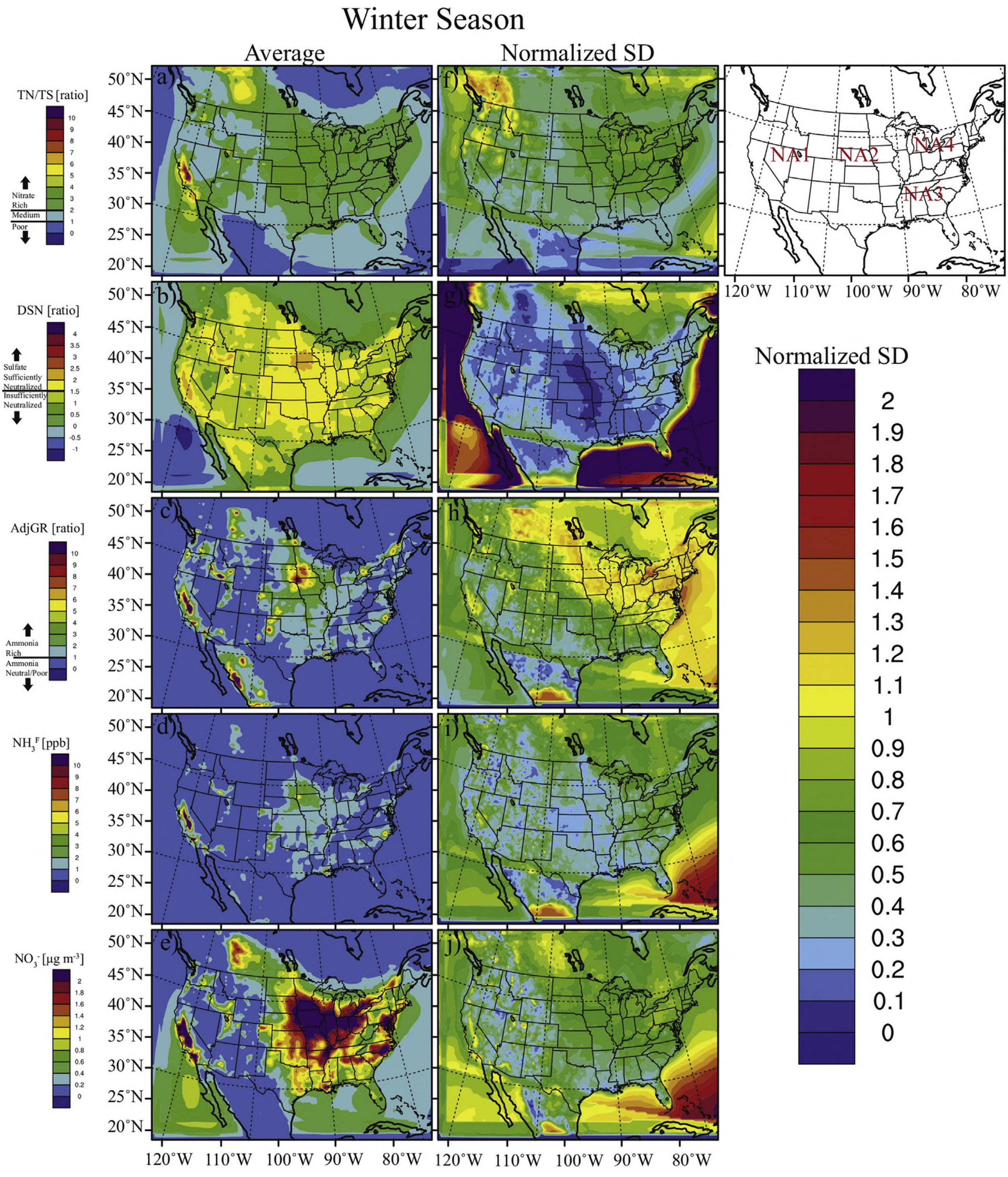

Fig. 5. Same as in Fig. 4, but for TN/TS, DSN, AdjGR, NH_3^F, and NO_3^- for the winter (DJF) season.

$PM_{2.5}$ NO_3^- formation is thermodynamically favored. On average, models predict NO_3^- medium (TN/TS = 1–2) to rich (TN/TS > 2) conditions across the U.S (Fig. 5a). Individual models agree that where SO_4^{2-} is fully neutralized, there is excess NH_3^F for $PM_{2.5}$ NO_3^- formation under cold temperatures (Figure S5) (Ansari and Pandis, 1998; Pinder et al., 2008). Average model results indicate that there is mainly sufficiently neutralized conditions, NH_3 rich conditions, and $PM_{2.5}$ sensitivity to TN changes in NA2 and NA3, while more NH_3 poor conditions (embedded with localized NH_3 rich), and $PM_{2.5}$ sensitivity to NH_3 changes in NA1 and NA4 (Fig. 5b–d). There is good inter-model agreement in DSN, with the lowest NSDs across NA/U.S. (Fig. 5g, Table 2); however, there is larger inter-model

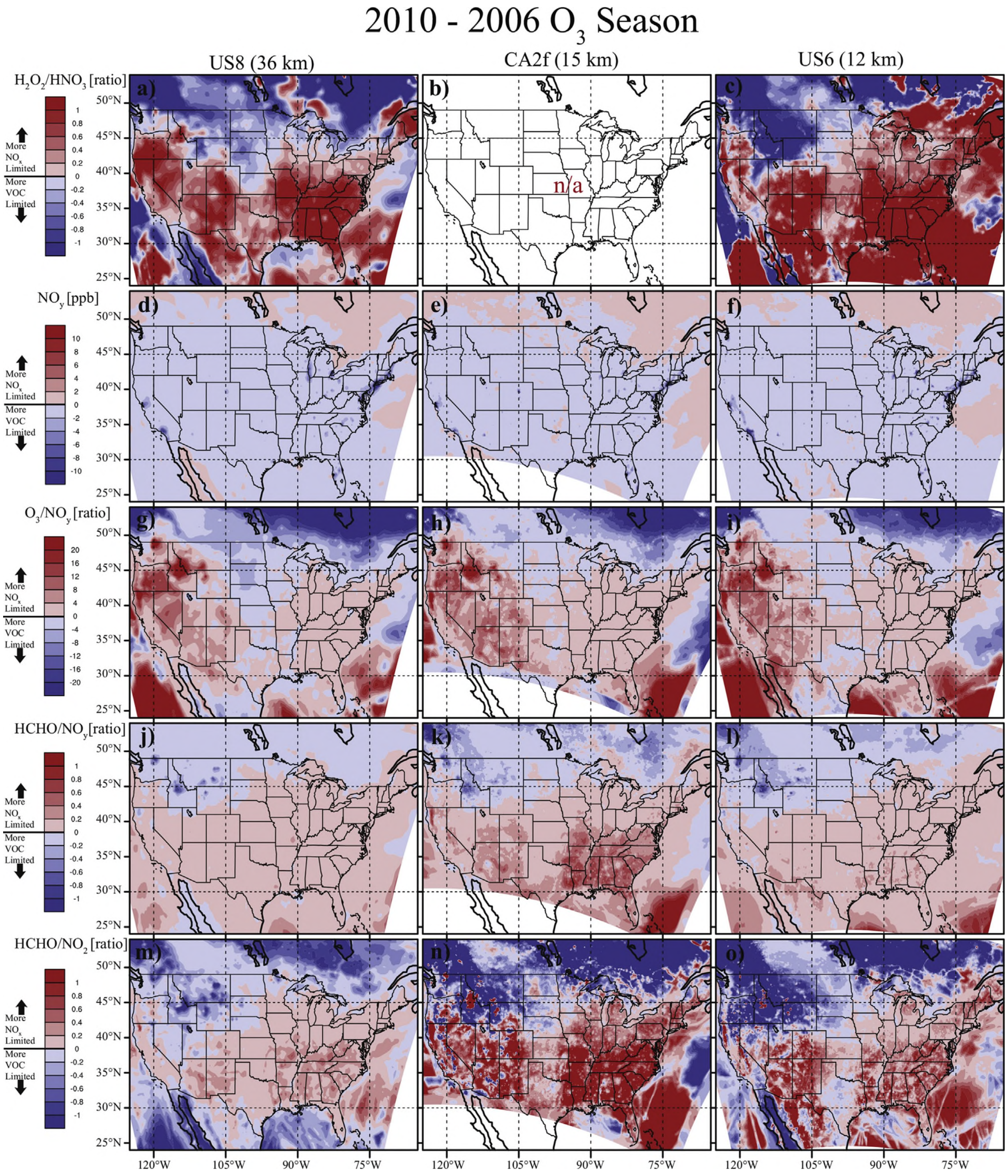

Fig. 6. Difference (2010–2006) plots representing changes in H_2O_2/HNO_3 (a–c), NO_y (d–f), O_3/NO_y (g–i), $HCHO/NO_y$ (j–l), and $HCHO/NO_2$ (m–o) for averaged afternoon hours during the O_3 season. NO_x-VOC-limited chemistry indicator changes are color shaded according to the legends on the left. (For interpretation of the references to color in this figure legend, the reader is referred to the web version of this article.)

variability for the other indicators, especially for TN/TS in parts of NA1 and NA4, and AdjGR in NA2 − NA4 (Fig. 5f and h). The NA/U.S. average NSD is over twice as large as that for DSN. The relatively larger inter-model variability in TN/TS in NA1 stems from inter-model differences in predicted SO_4^{2-} concentrations, as there is relatively smaller variability in NO_3^- concentrations in this region (Fig. 5j). In NA2 − NA4, the TN/TS and AdjGR variability stems from relatively different amounts of NO_3^- formation for some models under cold winter temperatures (Fig. 5e, j, and S5u–S5y). The models employ four different combinations for their inorganic aerosol, gas-, and aqueous-phase chemistry mechanisms (Table 1). Kim et al. (2011) and Y. Zhang et al. (2012b) indicated less than a 1% $PM_{2.5}$ concentration difference, but up to a 26% $PM_{2.5}$ composition difference from a comparison of models that used the same aerosol mechanism, but different gas-phase mechanisms. Furthermore, the reaction rate constant of SO_2 + OH is the same across all models, such that the larger inter-model variability in TN/TS in NA1, and TN/TS and AdjGR in NA2–NA4, are also likely impacted by different SO_2 (e.g., different plume rise calculations) or OH concentrations. Other impacts may also derive from different spatial resolutions. These lead to significant impacts on $PM_{2.5}$ sensitivity, e.g., the calculated average values of AdjGR over NA2–NA4 range from about 0.3 (NH_3 poor) − 1.4 (NH_3 rich) for the different models (Figure S5k–S5t). Overall, NA/U.S.-wide NSD averages in Table 2 indicate that there is relatively low inter-model variability for DSN (0.30), but larger variability for AdjGR (0.80). The lowest inter-model variability is for DSN in NA3 (0.23), while the largest is for AdjGR in NA4 (1.04). The larger inter-model variability for the surface $PM_{2.5}$ indicators, especially AdjGR, indicates that they are less robust than the surface O_3 indicators.

4.3. Changes in O_3 and $PM_{2.5}$ sensitivity from 2006 to 2010

Fig. 6 presents difference (2010–2006) plots for the five O_3 indicators to provide additional insight into changes in NO_x-VOC-O_3 sensitivity to emission and meteorological changes between the 2006 and 2010 O_3 season. The models indicate increases in all indicator ratios (Fig. 6a–c, g–i, and j–o) for southern NA1–NA2, and nearly all of NA3–NA4, along with NA/U.S.-wide decreases in NO_y (Fig. 6d–f). Analyses of the emissions support this finding, indicating NA/U.S.-wide decreases in summertime average NO_x daily emissions between 2006 and 2010, especially near point sources and urban centers (Pouliot et al., 2015; Stoeckenius et al., 2015; Yahya et al., 2015b). There is however a dipole in the sign of NO_x- and VOC-limited changes between northern NA1-NA2 and NA3. For NA1-NA2, further analysis of the meteorological IC-BCs show a decrease in mean summer surface temperatures, coincident with decreases in emissions of NO_x and anthropogenic VOCs of about −1000 and −4500 Mg day^{-1} respectively (Stoeckenius et al., 2015). Decreased temperature and resultant biogenic VOC emissions, occurring in tandem with relatively large anthropogenic VOC emission reductions compared to NO_x between 2006 and 2010, is conducive for increased VOC-limited conditions in NA1-NA2. Increased temperature, biogenic VOC emissions, and relatively large NO_x emission reductions of about −2000 Mg day^{-1} compared to VOC emissions of about −500 Mg day^{-1}, further increased the NO_x-limited conditions in NA3. Fig. 1 in Yahya et al. (2015b) supports our hypothesis, while indicating a similar dipole in 2006–2010 summertime VOC emission (anthropogenic + biogenic) changes, which was largely driven by temperature changes in NA1-NA2 and NA3. All three models shown in Fig. 6 indicate similar spatial patterns in the change in O_3 sensitivity in 2010 relative to 2006; however, there are differences in magnitude, especially for HCHO/NO_y and HCHO/NO_2 in NA1 and NA3. The larger in magnitude shift towards more NO_x-limited conditions for CA2f and US6 in NA3, compared to US8, is due to a combination of different responses from different biogenic emission models and versions (MEGAN vs. BEIS; Table 1) impacting isoprene emissions and resulting HCHO concentrations, different gas-phase chemistry mechanisms (CB05 vs. ADOMII; Table 1) that implement different VOC chemistry, and lower NO_x concentrations for the CA2f model specifically (Table S1 in Makar et al., 2015a). The policy implications from results in Fig. 6 are that 1) inter-model variability demonstrates a need for continued multi-model dynamic assessments of indicator sensitivities, which should be based on the most detailed current emission inventories as they become available every three years from NEI, while 2) enactment of individual state implementation plans following multi-model dynamic assessments are important to deriving state-specific NO_x-VOC policy for the appropriate control strategies of O_3 pollution.

Fig. 7 shows the changes in sensitivity for the $PM_{2.5}$ indicators TN/TS, DSN, AdjGR, and NH_3^F, as well as for NO_3^- concentration between 2006 and 2010. Supplementary Section 4.3 and Figure S6, provide additional details on the changes in sensitivity for the $PM_{2.5}$ indicator TA/TS, and for $PM_{2.5}$ species NH_4^+, SO_4^{2-}, and NO_3^- between 2006 and 2010. There is considerable spatial and inter-model variability in the changes in $PM_{2.5}$ sensitivity, such as in NA1, where there are large differences in the spatial distribution of increasing NO_3^- rich versus poor conditions (Fig. 7a–c), with less variability for changes in NO_3^- concentrations (Fig. 7m–o). The impact of TS is larger than TN on changes on TN/TS in NA1, where the regions of SO_4^{2-} decreases in NA1 correlate well with the TN/TS increases for winter 2006–2010 (Figure S6g–S6i). There are widespread increases in DSN across NA/U.S. for US6, due to more predominant increases in NH_4^+, in conjunction with less SO_4^{2-} increases compared to the other models, in spite of larger NO_3^- increases for US6. In NA1 − NA3, there are differences in response of AdjGR and NH_3^F for US8 (Fig. 7g and j), while indicating widespread decreases, as compared to increases for CA2f (Fig. 7h and k) and US6 (Fig. 7i and l). An interesting response is in central California, where all models have increased AdjGR under decreased NH_3^F, indicating that the increases in AdjGR are driven by local NO_3^- decreases, likely due to relatively large local wintertime NO_x emission decreases of about −1000 Mg day^{-1}, compared to minimal surface temperature changes and NH_3 and SO_2 emission decreases of about −100 Mg day^{-1} (Stoeckenius et al., 2015).

In NA2, the models agree for decreases in AdjGR due to increases in $PM_{2.5}$ NO_3^- concentrations, with CA2f and US6 indicating the largest $PM_{2.5}$ NO_3^- increase. In spite of decreases in NO_x emissions in NA2 of about −3000 Mg/day, significant surface temperature decreases in the region (exhibited in both the initial and modeled conditions) lead to increased $PM_{2.5}$ NO_3^- formation in the models, in agreement with analysis of $PM_{2.5}$ composition observations at the surface (Stoeckenius et al., 2015). In NA3, average surface temperature and NO_x emissions decrease in 2010 relative to their values in 2006. US6 predicts large increases in $PM_{2.5}$ NO_3^-, but CA2f and US8 predict smaller $PM_{2.5}$ NO_3^- increases or even decreases. Other instances of opposite $PM_{2.5}$ sensitivity changes include US8 predicting decreases in AdjGR and NH_3^F (shift towards more $PM_{2.5}$ sensitivity to NH_3) across many areas of NA/U.S., while CA2f and US6 oppositely predicting increases (shift towards more $PM_{2.5}$ sensitivity to TN) for these indicators. This is a result of the use of the gas-phase mechanism/aerosol module combination (CB05/MADE) used in US8, which is different than both CA2f (ADOMII/CAM) and US6 (CB05-TU/AERO6) responding differently to the predominant gas (SO_2, NO_x, and NH_3) emission decreases and temperature changes across NA/U.S. between winter 2006 and 2010 (Yahya et al., 2015a). In contrast to the other models, US8 predicts overall less increase (or more decrease) in NH_4^+ for all regions, however, with similar SO_4^{2-} increases, thus leading to

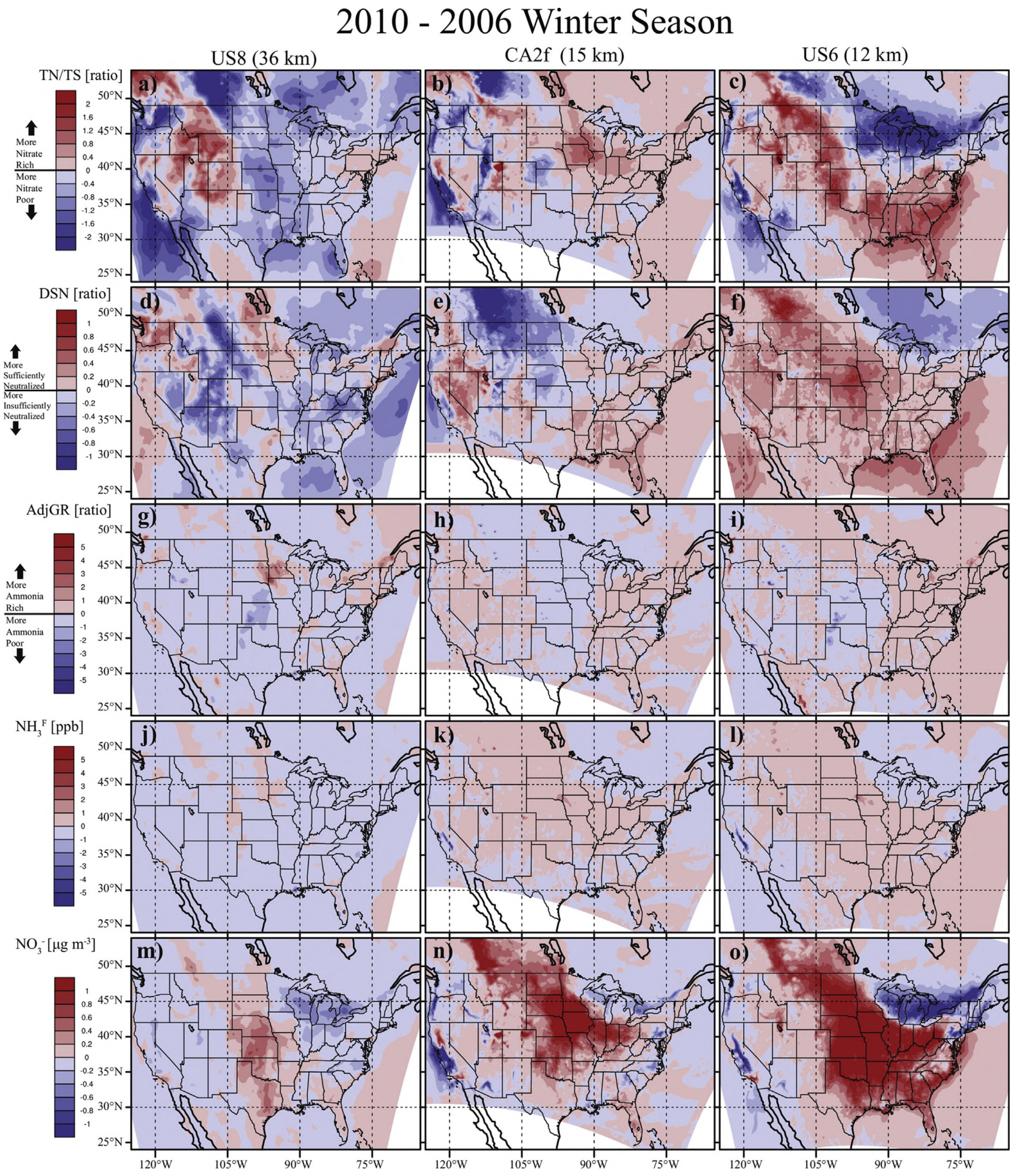

Fig. 7. Same as in Fig. 6, but for TN/TS (a–d), DSN (e–h), AdjGR (i–l), NH_3^F (m–p), and NO_3^-(q–t) changes for the winter (DJF) season.

predominantly decreasing TA/TS (Figure S6a–S6i), and corresponding decreases in NH_3^F and AdjGR. US8, CA2f, and US6 indicate progressively increased AdjGR in northeast NA4, due to progressively increasing TA/TS, and enhanced TA and NH_3^F in this region. There are clearly large ranges for different model responses of TN/TS, DSN, and AdjGR, which depend on specific gas-phase mechanism, aerosol module, spatial resolution, and region of NA/U.S. considered. Considering the large inter-model variability in $PM_{2.5}$ indicator sensitivity, caution must be used when using a single model prediction of changes in AdjGR to address the appropriate policy and control strategies for $PM_{2.5}$ pollution, i.e., the choice in implementing future measures to reduce either NH_3 or TN for different regions of the U.S in the winter.

5. Summary and conclusions

In the O_3 season, the six simulations that participated in this model inter-comparison predict similar values for H_2O_2/HNO_3, NO_y, and O_3/NO_y, while indicating dominant NO_x-limited chemistry for NA/U.S., except near urban centers that are predicted to be VOC-limited, especially by the higher resolution models. NOy and O_3/NO_y overpredict the extent of VOC-limited chemistry in the southeast U.S. (Fig. 1 and S1), but are more robust (smaller standard deviations and inter-model variability) compared to the H_2O_2/HNO_3, $HCHO/NO_y$, and $HCHO/NO_2$ (larger standard deviations and inter-model variability) indicators (Fig. 4). Larger differences arise for $HCHO/NO_y$ and $HCHO/NO_2$ due to dependencies on the model gas-phase mechanism (CBM vs. non-CBM), spatial resolution, and other differences such as the biogenic emissions model (Table 1). Additional work, however, comparing model response of these (and other) indicators to focused NO_x and VOC emission reductions, are needed before definite recommendations can be made. Additional measurements compared to further short-term diagnostic modeling, would provide even more vigorous evaluations outside of the southeast U.S. region, as well as lead to significant O_3 and $PM_{2.5}$ policy implications across the NA domain.

The SCIAMACHY comparison indicates that models tend to underpredict the $HCHO/NO_2$ column indicator in both the O_3 and non-O_3 season, with the exception of those models that had large underpredictions in NO_x concentrations (Fig. 3). Inter-model and SCIAMACHY observation comparisons also help put these models in context when they are used to develop effective O_3 control strategies across NA domain, while unveiling differences in using either a tropospheric column or surface $HCHO/NO_2$ indicator to diagnose the O_3 formation regime. Our results show that use of a column $HCHO/NO_2$ indicator leads to less VOC-limited regions near the urban centers, as well as more widespread NO_x-limited regimes compared to the surface $HCHO/NO_2$ indicator (Fig. 4 and S3). Furthermore, when models employ a combined Carbon Bond Mechanism, with the latest biogenic emission model, there are more consistent NO_x-limited predictions in surface $HCHO/NO_y$ and $HCHO/NO_2$ in the southeast U.S., but less consistent than other models in northwestern U.S., surrounding urban centers in northeast U.S., and in parts of Canada and Mexico, where emissions data are sparser (Figure S4).

In addition, we analyzed modeled $PM_{2.5}$ indicators over NA/U.S. in winter. Although there is a systematic underprediction in the degree of sulfate neutralization (DSN) (Fig. 2), it is currently a more robust (smaller standard deviations and inter-model variability) $PM_{2.5}$ indicator than the adjusted gas ratio (AdjGR) (larger standard deviations and inter-model variability), which exhibits a large range in predicted NH_3 poor ($AdjGR \leq 1$) versus NH_3 rich ($AdjGR > 1$) in the Midwest to northeast U.S. Such a model disparity in AdjGR, leads to a prediction of different NH_3 or TN sensitivities for the control of $PM_{2.5}$ concentrations in the winter. Furthermore in summer, all models perform poorly for AdjGR, indicating very large overpredictions in AdjGR and the extent of the NH_3 rich conditions here. This suggests that there is low confidence in modeled AdjGR for application to $PM_{2.5}$ control and policy strategies, and that more detailed diagnostic work is needed to determine the underlying mechanistic causes of these differences in model sensitivity.

Analyzing the inter-model comparison changes in O_3 and $PM_{2.5}$ sensitivity from 2006 to 2010 allows us to diagnose the responses of different models to changes in chemical emissions and meteorology. Increases in NO_x-limited conditions dominated across the U.S., especially near point sources, and are predicted by all models. The change is attributed to NO_x emission decreases in 2010 relative to the level in 2006. The three models also agree on the spatial distribution of change for O_3 indicator sensitivity, due to the relative surface temperature and emission changes between 2006 and 2010, while differences in the magnitude are attributed to different biogenic emission models and gas-phase chemistry impacts. This leads to policy implications regarding the need for continued multi-model assessments at the highest possible resolution, while using the most detailed emission inventories currently available. There is larger variability in the modeled change in $PM_{2.5}$ indicators, DSN and AdjGR, between 2006 and 2010, in part due to inter-model variability in the biogenic emissions, oxidation chemistry, and secondary organic aerosol abundance predicted by different model treatments (Table 1), which can in turn impact the response for the inorganic species. Thus compared to the O_3 indicators, the $PM_{2.5}$ indicators are currently less robust, while suggesting that further model development is needed in this area.

Acknowledgments

This study is funded by the National Science Foundation EaSM program (AGS-1049200). The following agencies have prepared the datasets used in this study: the U.S. EPA (North American emissions processing), Environment Canada, Mexican Secretariat of the Environment and Natural Resources (Secretaríde Medio Ambiente y Recursos Naturales-SEMARNAT) and National Institute of Ecology (Instituto Nacional de EcologíINE) (North American national emissions inventories), the European Center for Medium Range Weather Forecasting Global and Regional Earth-system (Atmosphere) Monitoring using Satellite and in-situ data (CA2fMWF/GEMS) project and Meteo France/Centre national de recherches météorologiques (CNRM-GAME) for the Monitoring Atmospheric Composition and Climate (MACC) IC/BCs. Meteorological IC/BCs are provided by the National Center for Environmental Protection. Ambient North American concentration measurements are provided by the SouthEastern Aerosol Research and Characterization (SEARCH) network. We also acknowledge the free use of tropospheric HCHO (version 12) and NO_2 column data (version 2.3) from the SCIAMACHY sensors, which are obtained from www.temis.nl.

We would also like to acknowledge high-performance computing support from Yellowstone by NCAR's Computational and Information Systems Laboratory, sponsored by the National Science Foundation, and Stampede, provided as an Extreme Science and Engineering Discovery Environment (XSEDE) digital service by the Texas Advanced Computing Center (TACC). The Technical University of Madrid authors thankfully acknowledge the computer resources, technical expertise and assistance provided by the Centro de Supercomputación y Visualización de Madrid (CESVIMA) and the Spanish Supercomputing Network (BSC).

The views expressed here are those of the authors and do not necessarily reflect the views and policies of the U.S. Environmental Protection Agency (EPA). This paper has been subjected to EPA review and approved for publication.

Appendix A. Supplementary data

Supplementary data related to this article can be found at http://dx.doi.org/10.1016/j.atmosenv.2014.12.026.

References

Abdul-Razzak, H., Ghan, S.J., 2000. A parameterization of aerosol activation 2. Multiple aerosol types. J. Geophys. Res. Atmos. 105 (D3), 6837–6844.

Ackerman, I.J., Hass, H., Memmesheimer, M., Ebel, A., Binkowski, F.S., Shankar, U., 1998. Modal aerosol dynamics model for Europe: development and first applications. Atmos. Environ. 32 (17), 2981–2999.

Ahmadov, R., et al., 2012. A volatility basis set model for summertime secondary organic aerosols over the eastern United States in 2006. J. Geophys. Res. 117, D06301.

Alapaty, K., et al., 2012. New Directions: understanding interactions of air quality and climate change at regional scales. Atmos. Environ. 49, 419–421.

Ansari, A.S., Pandis, S.N., 1998. Response of inorganic PM to precursor concentrations. Environ. Sci. Technol. 32, 2706–2714.

Appel, K.W., Pouliot, G.A., Simon, H., Sarwar, G., Pye, H.O.T., Napelenok, S.L., Akhtar, F., Roselle, S.J., 2013. Evaluation of dust and trace metal estimates from the Community Multiscale Air Quality (CMAQ) model version 5.0. Geosci. Model Dev. 6, 883–899.

Baklanov, A., et al., 2014. Online coupled regional meteorology-chemistry models in Europe: current status and prospects. Atmos. Chem. Phys. 14, 317–398.

Barkley, M.P., et al., 2013. Top-down isoprene emissions over tropical South America inferred from SCIAMACHY and OMI formaldehyde columns. J. Geophys. Res. 118, 6849–6868.

Bélair, S., Crevier, L.-P., Mailhot, J., Bilodeau, B., Delage, Y., 2003a. Operational implementation of the ISBA land surface scheme in the Canadian regional weather forecast model. Part I: warm season results. J. Hydrometeor. 4, 352–370.

Bélair, S., Brown, R., Mailhot, J., Bilodeau, B., Crevier, L.-P., 2003b. Operational implementation of the ISBA land surface scheme in the Canadian regional weather forecast model. Part II: cold season results. J. Hydrometeor. 4, 371–386.

Belair, S., Mailhot, J., Girard, C., Vaillancourt, P., 2005. Boundary layer and shallow cumulus clouds in a medium-range forecast of a large-scale weather system. Mon. Weather Rev. 133, 1938–1960.

Binkowski, F.S., Shankar, U., 1995. The regional particulate matter model: 1. Model description and preliminary results,. J. Geophys. Res. 100 (D12), 26191–26209.

Binkowski, F.S., Aranachalam, S., Adelman, Z., Pinto, J.P., 2007. Examining photolysis rates with a prototype online photolysis module in CMAQ. J. Appl. Meteorol. Climatol. 46, 1252–1256.

Boersma, K.F., Eskes, H.J., Brinksma, E.J., 2004. Error analysis for tropospheric NO_2 retrieval from space. J. Geophys. Res. 109, D04311.

Bohren, C.F., Huffman, D.R., 1983. Absorption and Scattering of Light by Small Particles. Wiley and Sons, New York, p. 530.

Bohren, C.F., Huffman, D.R., 1998. Absorption and Scattering of Light by Small Particles, second ed. Wiley, New York, p. 530. ISBN 0-471-29340-7, ISBN 978-0-471-29340-8.

Byun, D.W., Schere, K.L., 2006. Review of the governing equations, computational algorithms, and other components of the models-3 Community Multiscale Air Quality (CMAQ) modeling system. Appl. Mech. Rev. 59, 51–77.

Carlton, A.G., Bhave, P., Napelenok, S., Edney, E.O., Sarwar, G., Pinder, R.W., Pouliot, G., Houyoux, M., 2010. Model representation of secondary organic aerosol in CMAQ v4.7. Environ. Sci. Technol. 44 (22), 8553–8560. American Chemical Society, Washington, DC.

Chapman, E.G., Gustafson Jr., W.I., Barnard, J.C., Ghan, S.J., Pekour, M.S., Fast, J.D., 2009. Coupling aerosol-cloud-radiative processes in the WRF-chem model: investigating the radiative impact of large point sources. Atmos. Chem. Phys. 9, 945–964.

Chen, F., Dudhia, J., 2001. Coupling an advanced land-surface/hydrology model with the Penn State/US7 MM5 modeling system. Part I: model implementation and sensitivity. Mon. Weather Rev. 129, 569–585.

Clough, S.A., Shephard, M.W., Mlawer, J.E., Delamere, J.S., Iacono, M.J., Cady-Pereira, K., Boukabara, S., Brown, P.D., 2005. Atmospheric radiative transfer modeling: a summary of the AER codes. J. Quant. Spectrosc. Radiat. Transf. 91 (2), 233–244.

Dave, J.V., 1972. Development of Programs for Computing Characteristics of Ultraviolet Radiation. Final Report under Contract NAS5–21680, NASA Report CR-139134. National Aeronautics and Space Administration, Goddard Space Flight Center, Greenbelt, Maryland, p. 27. NTIS # N75-10746/6SL.

DeMore, W.B., Sander, S.P., Molina, M.J., Golden, D.M., Hampson, R.F., Kurylo, M.J., Howard, C.J., Ravishankara, A.R., 1988. Chemical Kinetics and Photochemical Data for Use in Stratospheric Modeling, Evaluation Number 8. National Aeronautics and Space Administration, Jet Propulsion Laboratory, California Institute of Technology, Pasadena, California, p. 266.

De Smedt, I., Müller, J.-F., Stavrakou, T., Van der, A.R., Eskes, H., Van Roozendael, M., 2008. Twelve years of global observations of formaldehyde in the troposphere using GOME and SCIAMACHY sensors. Atmos. Chem. Phys. 8 (16), 4947–4963.

Dennis, R., Fox, T., Fuentes, M., Gilliland, A., Hanna, S., Hogrefe, C., Irwin, J., Rao, S.T., Scheffe, R., Schere, K., Steyn, D., Venkatram, A., 2010. A framework for evaluating regional-scale numerical photochemical modeling systems. Eviron. Fluid Mech. 10 (4), 471–489.

Easter, R.C., Ghan, S.J., Zhang, Y., Saylor, R.D., Chapman, E.G., Laulainen, N.S., Abdul-Razzak, H., Leung, L.R., Bian, X., Zaveri, R.A., 2004. MIRAGE: model description and evaluation of aerosols and trace gases. J. Geophys. Res. 109.

Ek, M.B., Mitchell, K.E., Lin, Y., Rogers, E., Grunmann, P., Koren, V., Gayno, G., Tarpley, J.D., 2003. Implementation of Noah land surface model advances in the National Centers for Environmental Prediction operational mesoscale Eta model. J. Geophys. Res. 108, 8851.

Emmons, L.K., et al., 2010. Description and evaluation of the Model for Ozone and Related chemical Tracers, version 4 (MOZART-4). Geosci. Model Dev. 3, 43–67.

Fahey, K.M., Pandis, S.N., 2001. Optimizing model performance: variable size resolution in cloud chemistry modeling. Atmos. Environ. 35, 4471–4478.

Fast, J.D., Gustafson Jr., W.I., Easter, R.C., Zaveri, R.A., Barnard, J.C., Chapman, E.G., Grell, G.A., Peckham, S.E., 2006. Evolution of ozone, particulates and aerosol direct radiative forcing in the vicinity of Houston using a fully coupled meteorology-chemistry-aerosol model. J. Geophys. Res. 111, D21305.

Filion, L., et al., 2010. The Canadian regional data assimilation and forecasting system. Weather Forecast. 25, 1645–1669.

Foley, K.M., et al., 2010. Incremental testing of the Community Multiscale Air Quality (CMAQ) modeling system version 4.7. Geosci. Model Dev. 3, 205–226.

Fung, C.S., Misra, P.K., Bloxam, R., Wong, S., 1991. A numerical experiment on the relative importance of H_2O_2 and O_3 in aqueous conversion of SO_2 to SO_4^{2-}. Atmos. Environ. 25A, 411–423.

Galmarini, S., Rao, S.T., Steyn, D.G., 2012. Preface to AMQEII: an international initiative for the evaluation of regional-scale air quality models-phase 1. Atmos. Environ. 53, 1–13.

Gong, S.L., Barrie, L.A., Blanchet, J.-P., 1997. Modeling sea-salt aerosols in the atmosphere: 1. Model development. J. Geophys. Res. 102, 3805–3818.

Gong, S.L., Barrie, L.A., Lazare, M., 2003a. Canadian Aerosol Module (CAM): a size-segregated simulation of atmospheric aerosol processes for climate and air quality models 2. Global sea-salt aerosol and its budgets. J. Geophys. Res. 107, 4779.

Gong, S.L., et al., 2003b. Canadian Aerosol Module: a size-segregated simulation of atmospheric aerosol processes for climate and air quality models. 1. Module development. J. Geophys. Res. 108, 4007.

Gong, W., et al., 2006. Cloud processing of gases and aerosols in a regional air quality model (AURAMS). Atmos. Res. 82, 248–275.

Grell, G.A., Frietas, S.R., 2013. A scale and aerosol aware stochastic convective parameterization for weather and air quality modeling. Atmos. Chem. Phys. Discuss. 13, 23845–23893.

Grell, G.A., Peckham, S.E., Schmitz, R., McKeen, S.A., Frost, G., Skamarock, W.C., Eder, B., 2005. Fully coupled 'online' chemistry in the WRF model. Atmos. Environ. 39, 6957–6976.

Guenther, A., Karl, T., Harley, P., Wiedinmyer, C., Palmer, P.I., Geron, C., 2006. Estimates of global terrestrial isoprene emissions using MEGAN (Model of Emissions of Gases and Aerosols from Nature). Atmos. Chem. Phys. 6, 3181–3210.

Hammer, M.-U., Vogel, B., Vogel, H., 2002. Findings on H_2O_2/HNO_3 as an indicator of ozone sensitivity in Baden-Wurttemberg, Berlin-Brandenburg, and the Po valley based on numerical simulations. J. Geophys. Res. 107 (D22), 8190.

Hansen, D.A., Edgerton, E.S., Hartsell, B.E., Jansen, J.J., Kandasamy, N., Hidy, G.M., Blanchard, C.L., 2003. The Southeastern aerosol research and characterization study: part 1. Overview. J. Air Waste Manage. Assoc. 53, 1460–1471.

Hodzic, A., Jimenez, J.L., 2011. Modeling anthropogenically controlled secondary organic aerosols in a megacity: a simplified framework for global and climate models. Geosci. Model Dev. 4, 901–917.

Hollingsworth, A., et al., 2008. Toward a monitoring and forecasting system for atmospheric composition: the GEMS Project. Bull. Am. Meteor. Soc. 89, 1147–1164.

Hong, S.-Y., Noh, Y., Dudhia, J., 2006. A new vertical diffusion package with an explicit treatment of entrainment processes. Mon. Weather Rev. 134, 2318–2341.

Huijnen, V., et al., 2010. Comparison of OMI NO_2 tropospheric columns with an ensemble of global and European regional air quality models. Atmos. Chem. Phys. 10, 3273–3296.

Im, U., Bianconi, R., Solazzo, E., Kioutsioukis, I., Badia, A., Balzarini, A., Baro, R., Bellasio, R., Brunner, D., Chemel, C., Curci, G., Flemming, J., Forkel, R., Giordano, L., Jimenez-Guerrero, P., Hirtl, M., Hodzic, A., Honzak, L., Jorba, O., Knote, C., Kuenen, J.J.P., Makar, P.A., Manders-Groot, A., Neal, L., Perez, J.L., Pirovano, G., Pouliot, G., San Jose, R., Savage, N., Schroder, W., Sokhi, R.S., Syrakov, D., Torian, A., Tuccella, P., Werhahn, K., Wolke, R., Yahya, K., Zabkar, R., Zhang, Y., Zhang, J., Hogrefe, C., Galmarini, S., 2015a. Evaluation of operational online-coupled regional air quality models over Europe and North America in the context of AQMEII phase 2. Part I: ozone. Atmos. Environ. 115, 404–420.

Im, U., Bianconi, R., Solazzo, E., Kioutsioukis, I., Badia, A., Balzarini, A., Baro, R., Bellasio, R., Brunner, D., Chemel, C., Curci, G., Denier van der Gon, H.A.C., Flemming, J., Forkel, R., Giordano, L., Jimenez-Guerrero, P., Hirtl, M., Hodzic, A., Honzak, L., Jorba, O., Knote, C., Makar, P.A., Manders-Groot, A., Neal, L., Perez, J.L., Pirovano, G., Pouliot, G., San Jose, R., Savage, N., Schroder, W., Sokhi, R.S., Syrakov, D., Torian, A., Tuccella, P., Werhahn, K., Wolke, R., Yahya, K., Zabkar, R., Zhang, Y., Zhang, J., Hogrefe, C., Galmarini, S., 2015b. Evaluation of operational online-coupled regional air quality models over Europe and North America in the context of AQMEII phase 2. Part II: particulate matter. Atmos. Environ. 115, 421–441.

Inness, A., et al., the MACC team, 2013. The MACC reanalysis: an 8 yr data set of atmospheric composition. Atmos. Chem. Phys. 13, 4073–4109.

Janjic, Z.I., 2002. Nonsingular Implementation of the Mellor-Yamada Level 2.5 Scheme in the NCEP Meso Model, NCEP Off. Note, vol. 437. Natl. Cent. for Environ. Predict., College Park, Md, p. 61.

Jones, S., Creighton, G., 2011. AFWA dust emission scheme. In: 16th Weather Squadron Conference, Aerosols/Fine Scale and Ensemble Models, 23 June, 2011.

Kain, J.S., 2004. The Kain-Fritsch convective parameterization: an update. J. Appl. Meteorol. 43, 170–181.

Kain, J.S., Fritsch, J.M., 1990. A one-dimensional entraining/detraining plume model and its application in convective parameterizations. J. Atmos. Sci. 47, 2784–2802.

Kelly, J.T., Bhave, P.V., Nolte, C.G., Shankar, U., Foley, K.M., 2010. Simulating emission and chemical evolution of coarse sea-salt particles in the Community Multiscale Air Quality (CMAQ) model. Geosci. Model Dev. 3, 257–273.

Kim, Y., Sartelet, K., Seigneur, C., 2011. Formation of secondary aerosols: impact of the gas-phase chemical mechanism. Atmos. Chem. Phys. 11, 583–598.

Knote, C., et al., 2013. Simulation of semi-explicit mechanisms of SOA formation from glyoxal in a 3-D model. Atmos. Chem. Phys. Discuss. 13, 26699–26759.

Knote, Ch, Tuccella, P., Curci, G., Emmons, L., Orlando, J.J., Madronich, S., Baro, R., Jimenez-Guerrero, P., Luecken, D., Hogrefe, C., Forkel, R., Werhahn, J., Hirtl, M., Perez, J.L., San Jose, R., Giordano, L., Brunner, D., Khairunnisa, Y., Zhang, Y., 2015. Influence of the choice of gas-phase mechanism on predictions of key pollutants during the AQMEII phase-2 inter comparison. Atmos. Environ. 115, 553–568.

Kusaka, et al., 2001. A simple single layer urban canopy model for atmospheric models: comparison with multi-layer and slab models. Bound. Layer Meteor. 101, 329–358.

Li, J., Barker, H.W., 2005. A radiation algorithm with correlated k-distribution. Part I: local thermal equilibrium. J. Atmos. Sci. 62, 286–309.

Li, G., Lei, J., Prasad, C., 2012. Measurement of atmospheric formaldehyde profiles with a laser-induced fluorescence lidar. Proc. SPIE 8379 Laser Radar Technol. Appl. XVII, 83790I.

Liang, J.-Y., Jackson, B., Kaduwela, A., 2006. Evaluation of the ability of indicator species ratios to determine the sensitivity of ozone to reductions in emissions of volatile organic compounds and oxides of nitrogen in northern California. Atmos. Environ. 40, 5156–5166.

Lin, Y.-L., Farley, R.D., Orville, H.D., 1983. Bulk parameterization of the snow field in a cloud model. J. Clim. Appl. Meteor. 22, 1065–1092.

Liu, P., Zhang, Y., Yu, S.C., Schere, K.L., 2010. Use of a process analysis tool for diagnostic study on fine particulate matter predictions in the U.S. Part II: process analyses and sensitivity simulations. Atmos. Pollut. Res. 2 (1), 61–71.

Lowe, D.C., Schmidt, U., 1983. Formaldehyde (HCHO) measurements in the nonurban atmosphere. J. Geophys. Res. 88, 10844–10858.

Lu, C.-H., Chang, J.S., 1998. On the indicator-based approach to assess ozone sensitivities and emissions features. J. Geophys. Res. 103 (D3), 3453–3462.

Mailhot, J., Benoit, R., 1982. A finite-element model of the atmospheric boundary layer suitable for use with numerical weather prediction models. J. Atmos. Sci. 39, 2249–2266.

Mailhot, J., et al., 2006. The 15-km version of the Canadian regional forecast system. Atmos. Ocean 44, 133–149.

Makar, P.A., Gong, W., Hogrefe, C., Zhang, Y., Curci, G., Zabkar, R., Milbrandt, J., Im, U., Galmarini, S., Balzarini, A., Baro, R., Bianconi, R., Cheung, P., Forkel, R., Gravel, S., Hirtl, M., Honzak, L., Hou, A., Jimenez-Guerrero, P., Langer, M., Moran, M.D., Pabla, B., Perez, P.L., Pirovano, G., San Jose, R., Tuccella, P., Werhahn, J., Zhang, J., 2015a. Feedbacks between air pollution and weather, part 1: effects on chemistry. Atmos. Environ. 115, 499–526.

Makar, P.A., Gong, W., Hogrefe, C., Zhang, Y., Curci, G., Zabkar, R., Milbrandt, J., Im, U., Galmarini, S., Balzarini, A., Baro, R., Bianconi, R., Cheung, P., Forkel, R., Gravel, S., Hirtl, M., Honzak, L., Hou, A., Jimenez-Guerrero, P., Langer, M., Moran, M.D., Pabla, B., Perez, P.L., Pirovano, G., San Jose, R., Tuccella, P., Werhahn, J., Zhang, J., 2014b. Feedbacks between Air Pollution and Weather, Part 1: Effects on Weather. Atmos. Environ. 115, 442–469.

Martin, R.V., Fiore, A.M., Donkelaar, A.V., 2004. Space-based diagnosis of surface ozone sensitivity to anthropogenic emissions. Geophys. Res. Lett. 31, L06120.

Milbrandt, J.A., Yau, M.K., 2005a. A multimoment bulk microphysics parameterization. Part I: analysis of the role of the spectral shape parameter. J. Atmos. Sci. 62, 3051–3064.

Milbrandt, J.A., Yau, M.K., 2005b. A multimoment bulk microphysics parameterization. Part II: a proposed three-moment closure and scheme. J. Atmos. Sci. 62, 3065–3081.

Milford, J.B., Gao, D., Sillman, S., Blossey, P., Russell, A.G., 1994. Total reactive nitrogen (NO_y) as an indicator of the sensitivity of ozone to reductions in hydrocarbon and NO_x emissions. J. Geophys. Res. 99 (D2), 3533–3542.

Mlawer, E.J., Taubman, S.J., Brown, P.D., Iacono, M.J., Clough, S.A., 1997. Radiative transfer for inhomogeneous atmospheres: RRTM, a validated correlated-k model for the longwave. J. Geophys. Res. 102 (D14), 16663–16682.

Monin, A.S., Obukhov, A.M., 1954. Basic laws of turbulent mixing in the surface layer of the atmosphere (in Russian). Contrib. Geophys. Inst. Acad. Sci. USSR 151, 163–187.

Moran, M.D., et al., 2010. Particulate-matter forecasting with GEM-MACH15, a new Canadian air-quality forecast model. In: Steyn, D.G., Rao, S.T. (Eds.), Air Pollution Modelling and its Application XX. Springer, Dordrecht, pp. 289–292.

Morrison, H., Thompson, G., Tatarskii, V., 2009. Impact of cloud microphysics on the development of trailing stratiform precipitation in a simulated squall line: comparison of one- and two-moment schemes. Mon. Weather Rev. 137, 991–1007.

Nakanishi, M., Niino, H., 2004. An improved Mellor-Yamada Level-3 model with condensation physics: Its design and verification. Bound. Layer Meteor. 112, 1–31.

Odum, J.R., Jungkamp, T.P.W., Griffin, R.J., Flagan, R.C., Seinfeld, J.H., 1996. The atmospheric aerosol-forming potential of whole gasoline vapour. Science 276, 96–99.

Palmer, P.I., Jacob, D.J., Fiore, A.M., Martin, R.V., Chance, K., Kurosu, T.P., 2003. Mapping isoprene emissions over North America using formaldehyde column observations from space. J. Geophys. Res. 108.

Peterson, J.T., 1976. Calculated Actinic Fluxes (290–700 nm) for Air Pollution Photochemistry Applications. US Environmental Protection Agency Report Number US6-600/4-76-025, p. 55.

Pierce, T., Geron, C., Bender, L., Dennis, R., Tonneson, G., Guenther, A., 1998. Influence of increased isoprene emissions on regional ozone modeling. J. Geophys. Res. 103, 25611–25629.

Pinder, R.W., Dennis, R.L., Bhave, P.V., 2008. Observable indicators of the sensitivity of PM2.5 nitrate to emission reductions: part I. Derivation of the adjusted gas ratio and applicability at regulatory-relevant time scales. Atmos. Environ. 42 (6), 1275–1286.

Pleim, J.E., 2007a. A combined local and nonlocal closure model for the atmospheric boundary layer. Part I: model description and testing. J. Appl. Meteorol. Climatol. 46, 1383–1395.

Pleim, J.E., 2007b. A combined local and nonlocal closure model for the atmospheric boundary layer. Part II: application and evaluation in a mesoscale meteorological model. J. Appl. Meteorol. Climatol. 46, 1396–1409.

Pleim, J., Ran, L., 2011. Surface flux modeling for air quality applications. Atmosphere 2, 271–302.

Pleim, J.E., Xiu, A., Finkelstein, P.L., Otte, T.L., 2001. A coupled land–surface and dry deposition model and comparison to field measurements of surface heat, moisture, and ozone fluxes. Water Air Soil Poll. 1, 243–252.

Pouliot, G., Denier van der Gon, Hugo A.C., Kuenen, J., Zhang, J., Moran, M., Makar, P., 2015. Analysis of the emission inventories and model-ready emission datasets of Europe and North America for phase 2 of the AQMEII project. Atmos. Environ. 115, 345–360.

Rao, S.,T., Galmarini, S., Puckett, K., 2011. Air Quality Model Evaluation International Initiative (AQMEII): advancing the state of the science in regional photochemical modeling and its applications. Bull. Am. Meteor. Soc. 92, 23–30.

Sarwar, G., Luecken, D.J., Yarwood, G., 2006. Developing and implementing an updated chlorine chemistry into the Community Multiscale Air Quality Model. In: Presented at the 28th NATO/CCMS International Technical Meeting, Lepzig, Germany, May 15–19.

Sarwar, G., Bhave, P.V., 2007. Modeling the effect of chlorine emissions on ozone levels over the eastern United States. J. Appl. Meteorol. Climatol. 46, 1009–1019.

Sarwar, G., Fahey, K., Napelenok, S., Roselle, S., Mathur, R., 2011. Examining the impact of CMAQ model updates on aerosol sulfate predictions. In: The 10th Annual CMAS Models-3 User's Conference, October, Chapel Hill, NC.

Schell, B., Ackermann, I.J., Hass, H., Binkowski, F.S., Ebel, A., 2001. Modeling the formation of secondary organic aerosol within a comprehensive air quality model system. J. Geophys. Res. 106, 28275–28293.

Schere, K., et al., 2012. Trace gas/aerosol boundary concentrations and their impacts on continental-scale AQMEII modeling domains. Atmos. Environ. 53, 38–50.

Schwede, D., Pouliot, G.A., Pierce, T., 2005. Changes to the biogenic emissions inventory system version 3 (BEIS3). In: Proceedings of the 4th CMAS Models-3 Users' Conference, Chapel Hill, NC, 26–28 September 2005.

Shaw, W.J., Allwine, K.J., Fritz, B.G., Rutz, F.C., Rishel, J.P., Chapman, E.G., 2008. An evaluation of the wind erosion module in DUSTRAN. Atmos. Environ. 42, 1907–1921.

Sillman, S., 1995. The use of NO_y, H_2O_2 and HNO_3 as indicators for O_3-NO_x- VOC sensitivity in urban locations. J. Geophys. Res. 100, 14,175–14,188.

Sillman, S., 1999. The relation between ozone, NO_x and hydrocarbons in urban and polluted rural environments. Atmos. Environ. 33, 1821–1845.

Sillman, S., He, D., 2002. Some theoretical results concerning O_3-NO_x-VOC chemistry and NOx-VOC indicators. J. Geophys. Res. 107 (D22), 4659.

Sillman, S., He, D., Cardelino, C., Imhoff, R.E., 1997. The use of photochemical indicators to evaluate ozone-NO_x-hydrocarbon sensitivity: case studies from Atlanta, New York, and Los Angeles. J. Air Waste Manage. Assoc. 47, 642–652.

Sillman, S., He, D., Pippin, M., Daum, P., Kleinman, L., Lee, J.H., Weinstein-Lloyd, J., 1998. Model correlations for ozone, reactive nitrogen and peroxides for Nashville in comparison with measurements: implications for NO_x-hydrocarbon sensitivity. J. Geophys. Res. 103, 22,629–22,644.

Simon, H., Bhave, P.V., 2012. Simulating the degree of oxidation in atmospheric organic particles. Environ. Sci. Technol. 46, 331–339.

Skamarock, W.C., Klemp, J.B., Dudhia, J., Gill, D.O., Barker, D.M., Duda, M.G., Huang, X.-Y., Wang, W., Powers, J.G., 2008. A Description of the Advanced Research WRF Version 3. National Center for Atmospheric Research Tech. Note, US7/TN- 475+STR, p. 113.

Solazzo, E., et al., 2012a. Model evaluation and ensemble modelling of surface-level ozone in Europe and North America in the context of AQMEII. Atmos. Environ. 53, 60–74.

Solazzo, E., et al., 2012b. Operational model evaluation for particulate matter in Europe and North America in the context of AQMEII. Atmos. Environ. 53, 75–92.

Stockwell, W.R., Lurmann, F.W., 1989. Intercomparison of the ADOM and RADM Gas-phase Chemical Mechanisms. Electrical Power Research Institute Topical Report. Electrical Power Research Institute, 3412 Hillview Avenue, Palo Alto, CA, p. 401.

Stockwell, W.R., Middleton, P., Chang, J.S., Tang, X., 1990. The second generation regional acid deposition model chemical mechanism for regional air quality modeling. J. Geophys. Res. 95 (D10).

Stoeckenius, T., Chemel, C., Zagunis, J., Sakulyanontvittaya, T., 2015. A comparison between 2010 and 2006 air quality and meteorological conditions, and emissions and boundary conditions for the AQMEII-2 North American domain. Atmos. Environ. 115, 389–403.

Tie, X., Madronich, S., Walters, S., Zhang, R., Racsh, P., Collins, W., 2003. Effect of clouds on photolysis and oxidants in the troposphere. J. Geophys. Res. 108 (D20), 4642.

Tonnesen, G.S., Dennis, R.L., 2000. Analysis of radical propagation efficiency to assess ozone sensitivity to hydrocarbons and NO_x: 1. Local indicators of instantaneous odd oxygen production sensitivity. J. Geophys. Res. 105 (D7), 9213–9225.

van der A, R.J., Peters, D.H.M.U., Eskes, H.J., Boersma, K.F., Van Roozendael, M., De

Smedt, I., Kelder, H.M., 2006. Detection of the trend and seasonal variation in tropospheric NO_2 over China. J. Geophys. Res. 111, D12317.

van der A, R.J., Eskes, H.J., Boersma, K.F., van Noije, T.P.C., Van Roozendael, M., De Smedt, I., Peters, D.H.M.U., Kuenen, J.J.P., Meijer, E.W., 2008. Identification of NO_2 sources and their trends from space using seasonal variability analyses. J. Geophys. Res. 113, D04302.

Venkatram, A., Karamchandani, P.K., Misra, P.K., 1988. Testing a comprehensive acid deposition model. Atmos. Environ. 22, 737–747.

Vukovich, J., Pierce, T., 15–18 April 2002. The implementation of BEIS3 within the SMOKE modeling framework. In: Proceedings of the 11th International Emissions Inventory Conference, Atlanta, Georgia. Available at: www.epa.gov/ttn/chief/conference/ei11/modeling/vukovich.pdf.

Walcek, C.J., Taylor, G.R., 1986. A theoretical method for computing vertical distributions of acidity and sulfate production within cumulus clouds. J. Atmos. Sci. 43, 339–355.

Wang, K., Yahya, K., Zhang, Y., Hogrefe, C., Pouliot, G., Knote, C., San Jose, R., Perez, J.L., Guerrero, P.J., Baro, R., Makar, P., 2015a. A multi-model assessment for the 2006 and 2010 simulations under the Air Quality Model Evaluation International Initiative (AQMEII) phase 2 over North America: part II. Evaluation of column variable predictions using satellite data. Atmos. Environ. 115, 587–603.

Wang, K., Yahya, K., Zhang, Y., Wu, S.-Y., Grell, G., 2015b. Implementation and Initial Application of New Chemistry-Aerosol Options in WRF/Chem for Simulating Secondary Organic Aerosols and Aerosol Indirect Effects for Regional Air Quality. Atmos. Environ. 115, 716–732.

Wesely, M.L., 1989. Parameterization of surface resistances to gaseous dry deposition in regional-scale numerical models. Atmos. Environ. 23 (6), 1293–1304.

Wesely, M.L., Hicks, B.B., 2000. A review of the current status of knowledge on dry deposition. Atmos. Environ. 34, 2261–2282.

Whitten, G.Z., Heo, G., Kimura, Y., McDonald-Buller, E., Allen, D., Carter, W.P.L., Yarwood, G., 2010. A new condensed toluene mechanism for carbon bond: CB05-TU (2010). Atmos. Environ. 44, 5346–5355.

Wild, O., Zhu, X., Prather, M.J., 2000. Fast-J: accurate simulation of in- and below-cloud photolysis in tropospheric chemical models. J. Atmos. Chem. 37, 245–282.

Wong, D.C., Pleim, J., Mathur, R., Binkowski, F., Otte, T., Gilliam, R., Pouliot, G., Xiu, A., Young, J.O., Kang, D., 2012. WRF-CMAQ two-way coupled system with aerosol feedback: software development and preliminary results. Geosci. Model Dev. 5, 299–312.

Wuebbles, D.J., Hayhoe, K., 2002. Atmospheric methane and global change. Earth Sci. Rev. 57, 177–210.

Xiu, A., Pleim, J.E., 2001. Development of a land surface model. Part I: application in a mesoscale meteorological model. J. Appl. Meteorol. 40, 192–209.

Yahya, K., Wang, K., Gudoshava, M., Glotfelty, T., Zhang, Y., 2015a. Application of WRF/Chem over North America under the AQMEII Phase 2: Part I. Comprehensive evaluation of 2006 simulation. Atmos. Environ. 115, 733–755.

Yahya, K., Wang, K., Zhang, Y., Kleindienst, T.E., 2015b. Application of WRF/Chem version 3.4.1 over North America under the AQMEII Phase 2: evaluation of 2010 application and responses of air quality and meteorology-chemistry interactions to changes in emissions and meteorology from 2006 to 2010. Geosci. Model Dev. Discuss. 8, 1639–1686. http://dx.doi.org/10.5194/gmdd-8-1639-2015.

Yarwood, G., Rao, S., Yocke, M., Whitten, G., 2005. Updates to the Carbon Bond Chemical Mechanism: CB05. Final report to the U.S. US6, RT – 0400675.

Zaveri, R.A., Peters, L.K., 1999. A new lumped structure photochemical mechanism for large-scale applications. J. Geophys. Res. 104 (D23), 30387–30415.

Zaveri, R.A., Easter, R.C., Fast, J.D., Peters, L.K., 2008. Model for simulating aerosol interactions and chemistry (MOSAIC). J. Geophys. Res. 113, D13204.

Zhang, L., Gong, S.L., Padro, J., Barrie, L., 2001. A size-segregated particle dry deposition scheme for an atmospheric aerosol module. Atmos. Environ. 35, 549–560.

Zhang, L., Brook, J.R., Vet, R., 2002. On ozone dry deposition – with emphasis on non-stomatal uptake and wet canopies. Atmos. Environ. 36, 4787–4799.

Zhang, Y., 2008. Online coupled meteorology and chemistry models: history, current status, and outlook. Atmos. Chem. Phys. 8, 2895–2932.

Zhang, Y., Seigneur, C., Seinfeld, J.H., Jacobson, M., Clegg, S.L., Binkowski, F.S., 2000. A comparative review of inorganic aerosol thermodynamic equilibrium modules: similarities, differences, and their likely causes. Atmos. Environ. 34, 117–137.

Zhang, Y., Liu, P., Pun, B., Seigneur, C., 2006. A comprehensive performance evaluation of MM5-CMAQ for the summer 1999 southern oxidants study episode, Part I. Evaluation protocols, databases, and meteorological predictions. Atmos. Environ. 40, 4825–4873.

Zhang, Y., Vijayaraghavan, K., Wen, X.-Y., Snell, H.E., Jacobson, M.Z., 2009a. Probing into regional ozone and particulate matter pollution in the United States: 1. A 1 year CMAQ simulation and evaluation using surface and satellite data. J. Geophys. Res. 114, D22304.

Zhang, Y., Wen, X.-Y., Wang, K., Vijayaraghavan, K., Jacobson, M.Z., 2009b. Probing into regional ozone and particulate matter pollution in the United States: 2. An examination of formation mechanisms through a process analysis technique and sensitivity study. J. Geophys. Res. 114.

Zhang, Y., Wen, X., Jang, C., 2010. Simulating chemistry-aerosol-cloud-radiation-climate feedbacks over the continental US using the online-coupled Weather Research Forecasting Model with chemistry (WRF/Chem). Atmos. Environ. 44, 3568–3582.

Zhang, Y., Karamchandani, P., Glotfelty, T., Streets, D.G., Grell, G., Nenes, A., Yu, F., Bennartz, R., 2012a. Development and initial application of the global-through-urban weather research and forecasting model with chemistry (GU-WRF/Chem). J. Geophys. Res. 117.

Zhang, Y., Chen, Y.-C., Sarwar, G., Schere, K., 2012b. Impact of gas-phase mechanisms on weather research forecasting model with chemistry (WRF/Chem) predictions: mechanism implementation and comparative evaluation. J. Geophys. Res. 117, D1.